Universidade de Aveiro
2009

Depart. Engenharia Cerâmica e do Vidro

Ramkanna Venkatachalam

Estudos de sintonização do índice de refracção em filmes finos de di-ureasil Zr-oxo-aglomerados derivados de sol-gel

Refractive index tunability studies on sol-gel derived di-ureasil Zr-oxo-cluster thin films

Dissertação apresentada à Universidade de Aveiro (em conjunto com a Universidade de Augsburg, Alemanha) para cumprimento dos requisitos necessários à obtenção do grau de Mestre do programa FAME, realizada sob a orientação científica do Dr.Paulo André, Investigador Auxiliar do Instituto de Telecomunicações e Professor Auxiliar convidado da Universidade de Aveiro e Dr. Edison Pecoraro Investigador Auxiliar do Instituto de Telecomunicações.

A dissertation presented to the University of Aveiro (in co-ordination with University of Augsburg, Germany), in fulfilment of the requirements for the awarding of the FAME M.Sc program under the supervision of Dr. Paulo Andre, Invited Assistant Professor at the University of Aveiro and Assistant researcher from the Instituto de Telecomunicações and Dr. Edison Pecoraro, Assistant Researcher from Instituto de Telecomunicações.

Financial Support from European Union
FAME Master
An Erasmus Mundus program

Júri membros

Presidente	Professor Doutor.Vitor Brás de Sequeira Amaral, Departamento de Fisica, Universidade de Aveiro.
Arguente Principal	Professor Doutor. Manfred Niehus, Departamento de Engenharia de Electrónica e Telecomunicações e de Computadores Instituto Superior de Engenharia de Lisboa.
Orientador	Professor Auxiliar Doutor. Paulo Sergio de Brito André, Departamento de Fisica, Universidade de Aveiro, Investigador Auxiliar, Instituto de Telecomunicações.
Orientador	Doutor. Edison Pecoraro, Investigador Auxiliar, Instituto de Telecomunicações, Universidade de Aveiro.

Acknowledgements

I would like to express my sincere gratitude to all those who helped me in finishing my thesis work.

I deeply thank my advisors Dr. Luis Carlos, Dr. Paulo Andre and Dr. Maria Rute for their advices and their continuous encouragement. I am thankful to them for sharing their experience and supporting me throughout my work.

I would like to show my gratitude to Dr. Edison Pecoraro for his advices, support and guidance throughout the work. I would like to thank him for his patience, encouragement and knowledge sharing.

I would like to thank Mr. Carlos Vicente, PhD student, for his help during experiments and for his comments and suggestions. I would also like to thank Mr. Vasco Fernandes, Master student, for his comments and suggestions.

I thank Mr. João Prata, Lab incharge, for his support in the Institute of Telecommunication lab. I would like to thank Mrs. Celeste of Chemistry department for her help to make the UV-visible absorption spectrum measurements.

I sincerely thank the entire support given by Institute of Telecommunication and CICECO, University of Aveiro and to FCT Oreo2 project (PTDC-CTM-72093-2006).

I thank Prof. Ana Barros, Chemistry Department, FAME Master coordinator on her timely advices and encouragement. I would also like to thank Dr. Robert, FAME coordinator and Professors of Augsburg University, where I completed year one of the master program.

I deeply thank all the staffs in Augsburg University, University of Aveiro and Institute Polytechnic de Grenoble, who made my study and life abroad comfortable and easy.

I would like to show my gratitude for the financial support of FAME Master Erasmus Mundus program.

I would like to give my special thanks to my father, mother, all my family members, teachers and friends for their endless support.

Keywords Refractive index tunability, planar waveguide, organic-inorganic hybrid, sol-gel process, di-ureasil zirconium oxo-cluster thin films.

Summary

Planar optical waveguides are important element in optical telecommunication networks, being processed as integrated optical devices for efficient signal distribution. The main parameter to be considered for the waveguide production is its refractive index, which is dependent on the material composition. Hybrid material waveguides present refractive index tunability and can be processed at low cost, making them well suited for application in local area networks. To obtain integrated optical devices with the appropriate refractive index, it is necessary to know its dependency on the material composition and exposure to UV. In this study, organic-inorganic hybrid material di-ureapropyltriethoxysilane (d-U(600)) containing Methacrylic acid (MAA) and Zirconium (IV) tetrapropoxide, named as 'di-ureasil-zirconium oxocluster' have been synthesized using sol-gel method in various Si:Zr:MAA molar ratios and processed as thin films by spin coating. MAA is a UV photosensitive compound that changes its structure when irradiated, resulting in a phase change at molecular level. Prism coupler technique was used to measure the refractive index of the unexposed and UV exposed films. The basic aim of the thesis is to find the characteristic of the refractive index as function of Zr and MAA concentration and UV exposure time. The study guide us in choosing the optimal composition of materials and UV exposure time for processing devices with a particular refractive index. Results show, in samples without exposure to UV, there is higher tunable range of refractive index, by varying the Zr concentration, whereas, the MAA increase show a saturation behavior for refractive index change. Under UV irradiation, samples having Zr in various concentrations : diluted [Si:Zr(80:20)], intermediate [Si:Zr(60:40)] and concentrated systems [Si:Zr(40:60)] showed different behavior of refractive index change. The UV-Visible absorption spectra of the samples clearly show there is influence of Zr and MAA concentration on the absorption of the films under UV irradiation.

Palavras-chavas Sintonia do índice de refracção, guias de onda planares, híbrido orgânico-inorgânico, processo sol-gel, filmes finos de di-ureasil-zircónio oxo-aglomerados.

Resumo Os guias de onda ópticos são elementos importantes nas redes de comunicações ópticas sendo processados como dispositivos ópticos integrados para a eficiente distribuição de sinal. O principal parâmetro a ser considerado para a constução de um guia de onda é o seu índice de refração, que por sua vez dependente da composição do material do filme. Guias de onda realizados em materiais híbridos organicos-inorgânicos apresentam tunabilidade do índice de refracção e podem ser processados com baixo custo, fazendo com que sejam adequados para aplicação em redes locais de acesso. Para obter dispositivos ópticos integrados com a adequado índice de refração, é necessário conhecer a sua dependência com a sua composição do material e tempo de exposição UV. Neste estudo o material orgânico-inorgânico, di-ureiapropiltrietóxisilano (d-U(600)), contendo ácido metacrílico (MAA) e tetrapropóxido de zircónio (ZPO), denominado como "di-ureiasil zircónio oxo-cluster" foi sintetizado usando o método sol gel e processado em filmes finos através da técnica de deposição por rotação do substrato (spin coating). O MAA é um composto sensivel à radiação UV, que altera a sua estrutura quando irradiado, resultando numa mudança de fase ao nível molecular. A técnica de acoplamento por prisma foi usada para medir o índice de refração das amostras expostas e não expostas à radiação UV. O principal objectivo desta tese é determinar a dependência do índice de refracção em função da concentração de Zr e MAA e do tempo de exposição UV. Este estudo contribui para a escolha adequade para a composição do materials e do tempo de exposição UV, para o processamento de dispositivos. Os resultados mostram que em amostras não expostas à radiação UV, existe uma maior sintonio do índice de refração através da variação de Zr, por outro lado, o aumento da concentração de MAA conduz a uma saturação do valor do índice de refracção. Sob radiação UV, amostras com Zr em diferentes concentrações: diluído [Si:Zr(80:20)], intermédio [Si:Zr(60:40)] e sistema concentrado [Si:Zr(40:60)] apresentaram diferentes comportamentos da alteração de índice de refração, devido á exposição UV. O espectro de absorção UV-Visível das amostras mostra claramente que as concentrações de ZPO e MAA influenciam, a absorção dos filmes sob irradiação UV.

TABLE OF CONTENTS

LIST OF SYMBOLS

c	-	speed of light in vaccum
V_i	-	beam phase velocity in airgap
n_p	-	prism refractive index
ϕ	-	angle of beam over prism base
ϕ_m	-	angle measured for each mode
V_m	-	beam phase velocity in waveguide
N_m	-	effective refractive index
A	-	prism base angle
λ	-	wavelength
t	-	film thickness
ϕ_s	-	phase change in film substrate
ϕ_e	-	phase change in the air gap
n_f	-	refractive index of film
n_s	-	refractive index of substrate
m	-	mode number
σ	-	surface tension

LIST OF ABBREVIATIONS

ORMOCER	-	Organically modified polymer
ORMOSIL	-	Organically modified silica/silicate
PMMA	-	Poly(methymethacrylate)
d-U(600)	-	di-ureasil
d-UZ(600)	-	di-ureasil methacrylic acid modified zirconium oxo-cluster
d-UPTES	-	Ureapropyltetraethoxysilane
ICPTES	-	3-isocyanatopropyl-triethoxysilane
ZPO/$Zr(OPr^n)_4$	-	Zirconium tetra-propoxide
MAA	-	Methacrylic acid
Zr-OMc	-	MAA-modified $Zr(OPr^n)_4$
THF	-	Tetrahydrofuran
BtOH	-	Butanol
UV	-	Ultraviolet
TIR	-	Total internal reflection
IPN	-	Interpenetrating networks
TEOS	-	Tetraethoxysilane
TMOS	-	Tetramethoxysilane
Si-OH	-	Silanol group
pH	-	Power of hydrogen
DRO	-	Digital read out unit
DF	-	Dichroic film
IO	-	Integrated optics
RI	-	Refractive index error
STD	-	Standard deviation
R.H.S/L.H.S	-	Right/Left hand side
KK	-	Kramers-Kronig

LIST OF FIGURES

LIST OF TABLES

1. INTRODUCTION

1.1 Motivation

Optical fibers and integrated optical (IO) devices are required as basic elements in optical telecommunication networks. Integrated optical devices can be classified into passive, active, opto-electronic and electro-optical devices [1]. Passive optical devices such as splitters, filters, multiplexers, de-multiplexers are being used in an optical network especially in local area networks, where the dissemination of signal must be done at low price. These devices have more advantages than the copper based interconnects such as larger bandwidth, lower coupling losses, smaller size, lower weight, low power consumption and higher immunity to electromagnetic interferences. The technological perspectives for the IO devices also indicate that one of the possible utilization is on the implementation of low cost passive all-optical networks operating at high bit rate optical signals, bringing the optical fiber into the home of the subscriber [2]. Planar waveguides are the basic elements of the IO devices which must be available with low cost. For this purpose, there is the need to choose the best available materials to produce efficient waveguide to be processed as IO devices. Therefore it is very important to study the properties and processing of the available optical materials that can be used to fabricate high efficient IO devices. For any waveguide optical device, the study of the material's refractive index is important. This is due to the fact that the principle of wave-guiding is governed by the wave-guiding and the surrounding material's (substrate) refractive indices. Another key point is that, integrated optical devices must have refractive index that match the refractive index of the optical fibers, for efficient transmission of the data signals between these two mediums. Therefore, the study on the refractive index of materials is a relevant aspect in the design of these devices.

For high efficient optical integrated system, there is a need for devices with different functionalities. The materials for this purpose must have easiness in its processing including the property of photosensitivity to obtain various shapes of devices for the requisite functionality in the integrated optical system. The devices such as filters, couplers, etc., must have matching refractive index (compatible properties with the devices in the existing network) with the optical fibers that are already in use in the optical telecommunication network, which are normally silica based fibers having refractive index

value of around 1.5. The matching refractive index will minimize the absorption losses. The devices must possess very low absorption (attenuation) values at wavelengths that are used in the system. The most widely used wavelength for optical communication is 1.5μm. Integration of these devices with opto-electronic, electro-optic and electronic systems is highly preferable. To meet all the requirements, the materials considered for functional device processing must have tailor made properties with which devices having required optical properties (such as high transparency, matching refractive index, necessary thickness for total internal reflection, etc), good mechanical property (flexibility, etc), excellent thermal stability (stability to environment conditions namely temperature variation) and better chemical property (chemical inertness, resistance to water, adhesive to substrate, etc) can be attained. Materials used and devices fabricated must meet such requirements for applications in optical integrated circuits [1][2][3][4].

Silica based devices used in long range networks are costly and cannot be considered for local area networks [3]. Polymer (organic material) based devices are considered to be used in home based networks with additional advantages, as compared to silica based devices [3]. These materials have few disadvantages. The organic-inorganic hybrid materials can overcome some of the inorganic material's disadvantages such as low mechanical flexibility and high brittleness and also of the organic material's disadvantages such as low heat and water resistance [4]. Among the huge quantity of available precursor, the combination of organic-inorganic hybrids with methacrylic acid (MAA) modified metal oxide precursors(namely Zirconium tetrapropoxide, $Zr(OPr^n)_4$) has been recursively used for the production of low cost IO devices. Studies on the hybrid material named 'di-ureasil zirconium oxo-cluster'(d-UZ(600)) shows that it can be used to process planar waveguide as well as channel waveguides by direct writing with help of UV [2]. The blend of two hybrid materials namely d-UPTES (ureapropyltriethoxysilane) and methacrylic acid modified zirconium oxo-cluster (ZrOMc) makes it advantageous for varying the optical properties (especially the refractive index) of the system. It is done by varying the concentration of the precursors as well as using methacrylate photopolymerization under UV irradiation.

1.2 State of the art

Organic-inorganic hybrid (ORMOCER/ORMOSIL) materials have shown potential to be used in the production of optical waveguides, for applications such as optical interconnects for telecommunication, chemical sensing, bio-chemical sensing and opto-electronic devices [5] [6]. For the processing of integrated optical devices with various functionalities, different kinds of organic-inorganic hybrid materials have been found and are under research for attaining improved efficiency in all aspects [2]. Organic-inorganic materials composing of organo-functional siloxane oligomers prepared from alkyl- and/or aryl- alkoxysilanes and metal alkoxides in use for processing of these materials. In combination with Lanthanide ions and photopolymerizable polymers they offer a lot for tuning the properties of optical devices. From the available organic-inorganic hybrid materials under research some has been considered for waveguide fabrication, such as d-UPTES (di-ureasil) [4], MAPTMS (methacryloxypropyltrimethoxysilane) [4], and MEMO (3-methacryloxypropyltrimethoxysilane) [7]. Various processing techniques such as sol-gel, chemical vapor deposition, flame hybrolysis deposition, reactive ion etching, ion implantation, ion-exchange, sputtering, photolithography, moulding, phase mask technique, photobleaching, UV direct writing, electron-beam direct writing, and proton beam writing are used to prepare optical waveguides based on silica and polymers such as PMMA (Poly-methymethacrylate), fluorinated polymides, etc [3] [8] [9]. Among these techniques the conventional sol-gel processing is the highly preferred and advantageous method for processing organic-inorganic hybrid materials. Sol-gel processing along with techniques such as direct UV writing, electron-beam writing, phase masking offers a low temperature, photoimageable, low shrinkage production of optical waveguides with good optical and mechanical properties at low cost [4] [6].

Waveguide properties namely the refractive index, is considered critical for any optical device. The basic techniques for refractive index measurements are ellipsometry, prism coupler and interferometry [10][11]. Among these, prism coupler technique offers simple refractive index measurement of moderate to bulk thin films, obtained with reasonable low cost equipment. Commercial instruments based on the prism coupler method are available commercially and are used widely in laboratories [12]. In this thesis we reported the preparation of d-UZ(600) made thin films by sol-gel and spin coating, to

study the tunability of refractive index of optical thin films as function of material concentration and UV exposure time. Homemade UV chamber was used to expose the films to UV irradiation. The refractive index of all the films was measured by the prism coupler technique along with a software application (as calculation could not be done analytically).

1.3 Objectives of the thesis

The main objective of the thesis is to correlate the refractive index of the thin films as function of Zr and MAA concentration and the UV exposure time. The study of refractive index dependency can be divided into the following:

- Dependence of n with respect to Zirconium concentration.
- Dependence of n with respect to Methacrylic acid concentration.
- Dependence of n with respect to UV exposure.

Previous studies showed that the thin films made of d-UZ (600) are well suited for application in optical telecommunication as planar and UV patternable waveguides [2]. The study of refractive index dependency on Zr and MAA concentration and UV exposure time will give the right combination of the precursor concentration suitable for processing UV patternable planar waveguides with controllable refractive index for IO device fabrication.

1.4 Thesis structure

Chapter 1 of this thesis presents the work motivation. Chapter 2 provides the fundamentals of the processes and techniques used for the work. Chapter 3 deals with the experimental procedure carried out in the laboratories for processing thin films and measuring refractive indices. In chapter 4 the results and discussions of the work is done. Finally, chapter 5 deals with the conclusion of the work and suggestions to future activities.

1.5 Contribution

This work was presented during the First EMMI/FAME Education, Research and Training Meeting held at Bordeaux in July 2009. A technical paper is proposed to be published based on this thesis outcome.

2. THEORY

2.1 Optical Waveguides

Optical waveguides are the basic blocks of integrated optical devices [1]. This section deals with the basic geometry classification of optical waveguides, figure 2-1 shows the basic structure of an optical waveguide. The principle that governs the transmission of electromagnetic waves (light waves) inside a multimode waveguide is the total internal reflection (TIR). To occur a TIR inside a waveguide, the refractive index of waveguide material must be greater than the refractive index of cladding material (usually air) and the refractive index of the substrate. Light guiding is also affected by the thickness of the waveguide, since TIR takes place only at certain propagation angles (measured with interface normal) which are greater than a critical angle [13].

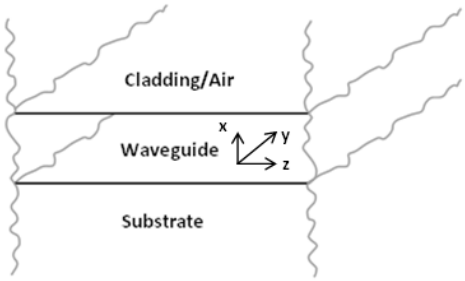

Figure 2-1 Basic structutre of optical waveguide [13].

Figure 2-2 displays the basic forms of a waveguide. 2-D and 3-D waveguides are the main types of waveguides found in a integrated optical circuit.

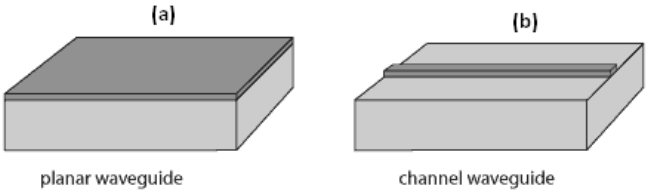

Figure 2-2 (a) 2-D (planar) waveguide (b) 3-D (channel) waveguide [14].

In 2-D waveguides (planar/slab waveguide), waves are confined only in one direction, this causes originates an expansion of the beam width due to diffraction. In 3-D waveguides (channel waveguide), light is confined in two directions. In addition to the straight 3-D waveguides shown in figure 2-2(b), there are other types of 3-D waveguides.

For example, corner-bent waveguide (change optical-path direction), bent and S-shaped waveguides, tapered waveguides (for smooth expansion of the guide width without mode conversion), branching waveguides (used for both dividing and combining optical power), crossed waveguides and directional waveguide couplers (for distributed mode coupling) [15]. In a optical integrated circuit these shapes are used to implement devices with the capacity to multiplex, de-multiplex or couple optical signals. Planar optical waveguide are also used in combination with gratings to produce wavelength filters. The organic-inorganic hybrid processing techniques provide incredible flexibilty to fabricate all type of waveguide devices for use in integrated optical circuits.

2.2 Hybrid materials

The initial origin of the hybrid material is unknown. But it is well known that the mixing of organic and inorganic compounds was carried out in ancient world for production of colorful and bright paints. These organic-inorganic mixed compounds are in recent times called as hybrid materials. The advanced study into materials derived from organic and inorganic mixtures has given birth to variety of hybrid materials for various applications [16].

The limitation of classical materials for different technological application such as optics, sensor technology, catalysis, ceramics, etc., has already been reached. This leads to a demand for tunability in the material property to expand the limitations and make it limitless for application purpose. Among the class of materials which have the ability to push the limit for specified application are the organic-inorganic hybrid materials. The hybrid material system combines the property of organic and inorganic materials giving an edge in tailoring the material property for various application by altering the component's composition and its structure at molecular scale [16].

Hybrid materials are basically classified on their species interactions. Hybrids showing weak interaction (Van der Waals, Hydrogen bonding or weak electrostatic interactions) are classified as Class-I. They include materials named as blends and interpenetrating network. Blends have inorganic components entrapped in the organic phase of the system. Interpenetration networks (IPN) have inorganic and organic components interpenetrated with strong chemical interactions. Figure 2-3 a) and b) shows

the Class-I type of hybrid material. Hybrids having strong interaction especially covalent bonding between clusters of inorganic compound and the organic compound (or) between inorganic and organic species are termed as class-II hybrids as shown in figure 2-3 b) and 2 c). The material dealt in the thesis comes under the class-II hybrids. Apart from classification based on interactions, hybrid materials are also classified based on structures. Structurally grouped compounds are named with respect to the reaction between the species as network modifier (inorganic network is modified by organic group), network builder (inorganic group forms an integral part of the system anchoring to organic phase of the system), and network functionalizer (a reactive functional group is incorporated in the system) [16].

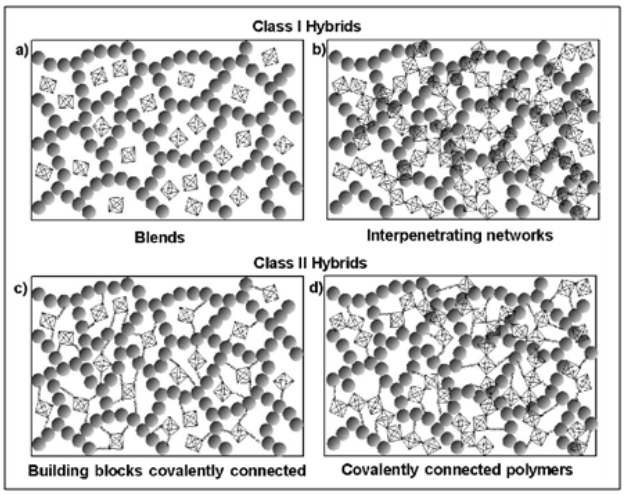

Figure 2-3 Types of hybrid material: (a) blends, (b) interpenetrating networks, (c) building blocks covalently connected, (d) covalently connected polymers [16].

Organic–inorganic materials offer promising properties for use as planar waveguides and as other systems in optical communication. They offer the control of refractive indices and thicknesses, thermo-stability, good miscibility, low shrinkage, and high optical transparency [17]. One of the main feature of using hybrids for optical telecommunication components is its ability to couple with silica based fibers and plastic optical fibers reducing the losses in the network. Other main feature of the hybrid material is that it can be tailored to contain photo-polymerisable system which helps to change the system refractive indices to our necessity. Hybrid materials have the potential to be used in waveguides for integrated optics especially for local area networks based on optical

communication, due to its advantages over organic based devices and inorganic based devices. The demand for providing cheap and faster optical communication at houses and at customer ends are growing higher. The application of hybrid materials in optical network systems will help to meet these demands. Also the hybrid materials feature of modifying the system at its molecular level, help tune the properties of optical devices giving lot of opportunities for various applications [16].

2.3 d-UZ(600) hybrids for optical telecommunication application

Di-ureasil Zr-oxo-cluster (d-UZ(600)) hybrid material, for which the refractive index study is done in this work, results from combination of d-UPTES (ureapropyltriethoxysilane) with MAA modified Zr-oxo-cluster (MAA+ZPO).

- *d-UPTES system*

The di-ureasil hybrid material is one of few hybrid materials under study for many years for use as host material in fabricating optical waveguides and other integrated optic systems. Planar waveguides prepared using d-UPTES, showed acceptable transparency, mechanical flexibility and thermal stability along with low propagation losses [4][18].

Figure 2-4 shows the d-UPTES structure. As shown, it is formed by poly (ether) based chains of variable length attached to urea cross linkages containing siliceous backbone at both ends [4][18]. The experimental preparation is given in section 2.

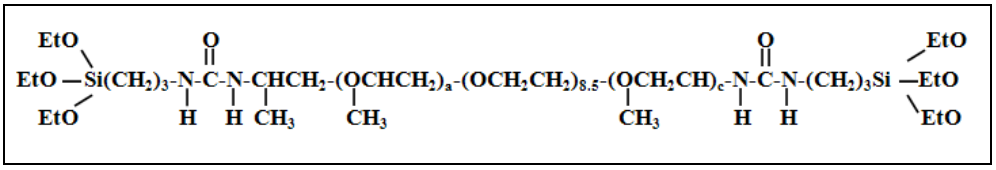

Figure 2-4 di-ureasil (d-UPTES).

- *Methacrylate modified Zr-oxo-cluster*

The incorporation of ZPO modified by MAA into the d-UPTES system, especially the presence of Zirconium helps in adjusting the refractive index of the host material as well as adds up to the systems optical properties at certain concentrations. MAA stabilizes the ZPO precipitation, since zirconium tetrapropoxide is sensitive to moisture which causes it to oxidize forming precipitates. The methacrylic acid addition is done to make the

system sensitive to UV exposure allowing the formation of photo-patternable waveguides. This occurs due to polymerization of the organic compound (methacrylate) present in the system. As the size and shape of the oxoclusters can be modified at its molecular level, we can change the concentrations to tailor the physical and chemical properties changing its size and shape [19]. Figure 2-5 shows the clusters being covered by chelating and bridging methacrylate ligands formed by the chemical reaction between zirconium tetrapropoxide and methacrylic acid. The structures of two different clusters of Zr are represented by ball and stick diagram in the figure. The figures adjacent to the ball and stick model shows the linkage of the coordination polyhedra (only the metal and oxygen atoms are shown in these representations) [20]. In this work the effect of cluster concentration on the refractive index is studied and the results showed that varying the cluster concentration, by changing the Zr and MAA concentration, the refractive index of hybrid system could be changed.

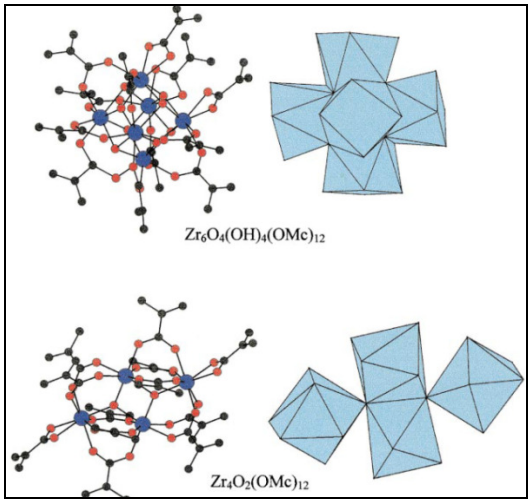

Figure 2-5 Structure of Zr-oxo-clusters [20].

[Blue ball - Zirconium, Red ball - Oxygen, Black ball - Organic compound]

The reactions which occur when zirconium tetrapropoxide and methacrylic acid are mixed together for the hybrid cluster formation are given below, adopted from study by Ulrich Schubert [19].

In the first step alkoxide ligands are replaced by carboxylate groups,

$$Zr(OPr^n)_4 + 2MAA \rightarrow Zr(OPr^n)_2 (OMc)_2 + 2PrOH \quad \text{-- (1)}$$

In the second step the liberated alcohol undergoes esterification reaction forming esters,

$$PrOH + MAA \rightarrow McOPr + H_2O \quad \text{-- (2)}$$

In the third step the water produced during the previous reaction together with the ester serves to hydrolyze the remaining alkoxide groups and acts as the source of oxide or hydroxide groups in the clusters. The very slow production of water allows a very controlled growth of the carboxylate substituted oxometalate clusters.

$$6Zr(OPr^n)_2\,(OMc)_2 + 8H_2O \rightarrow Zr_6(OMc)_{12}O_4(OH)_{12} + 12PrOH \quad \text{-- (3)}$$

- *Study on d-UZ (600) system*

Studies on the structural and optical properties of the diureasil zirconium oxo-cluster system showed there is considerable potential of d-UZ (600) for the development of passive and active integrated optical devices [4]. The synergism between the d-U(600) and MAA modified Zr-oxocluster hybrid systems allow them to be used for the production of various IO devices with different functionalities. Addition of d-UPTES to methacrylic acid modified ZPO will result in d-UZ(600) hybrid system containing Si and Zr nanobuilding blocks embedded in the organic phase of the system [2][18].

In a previous work, it was found that in a d-UZ (600) system there is effective interaction between the Zirconium nanodomains and the Silicon nanodomains in the system [18]. The Si and Zr nanobuilding blocks (NBB) are found to be dispersed in the organic phase [18]. The intercorrelation distances between the Si based NBB was found to be 26±1Å in d-U(600) and for Zr NBB it was 16±1Å in system containing $Zr(OPr^n)$ along with methacrylic acid in ratio 1:1. In the d-UZ(600) system the distance between NBB increased with the concentration of Zr-oxo-cluster. It increased from 18 to 25Å for Si NBB and 14 to 23Å when the Zr% was increased from 5 to 75 respectively [18]. This showed that the Si and Zr clusters are inter-constrained. Zr-OMc (Methacrylic acid modified Zr oxocluster) was found to be present over whole range of the composition. At lower concentrations of Zr it was seen that the clusters were well dispersed in UPTES and at higher concentrations segregation effect was noticed. The structural analysis also showed that the heterocondensation leading to Zr-O-Si is absent in the system. The study on the d-UZ (600) system exposed to UV showed that, there is change in the optical property of the system due to the Zr-OMc polymerization [2][4]. The variation, behavior and properties of cluster concentrations are studied by XRD (X-ray diffraction, SAXS (Small angle X-ray

scattering), FT-IR (Fourier transform - Infra red spectroscopy), FT-Raman (Fourier transform - Raman spectroscopy), and NMR (Nuclear magnetic resonance), Differential scanning calorimeter and Thermo gravimetric analysis techniques.

- *Cluster concentration influence on refractive index*

The cluster concentration can be varied by varying the molar concentration ratio of MAA to zirconium propoxide in d-UZ(600). The cluster concentration is directly proportional to the refractive index. By Mosotti-Clausius and Lorenz-Lorenz equation we can clearly state that increase in concentration of molecules leads to increase in refractive index [21]. As well it clearly gives the relation of refractive index with polarizability of compounds. As concentration of molecules changes, polarizability of atoms is also directly proportional to refractive index. Reactions leading to variable anion polarization in the system mainly contribute to refractive index change. From earlier studies on clusters we know changing the ratio of ZPO and MAA, the cluster size, the shape, the number of functional and non-functional cappings changes can be altered [20]. The changes in oxygen anion polarization can be expected due to the structural changes resulting because of the above said reasons. The study done by L.H. Ahrens shows that anion polarization has higher influence on refractive index [22].

2.4 Sol-gel process

The technique designated as sol-gel process is being used in various industries to process dense films, ceramic fibers, aerogels, thin film coatings, etc., for different applications. The process is well opted for the preparation of hybrid materials for optical telecommunication application, since the materials can be prepared at low cost and in low temperature making it suitable for production of optical waveguides and functional integrated optics. It also offers compositional and micro-structural control of the material which helps in altering the material optical property [23][24].

Sol-Gel process involves the formation of colloidal particles leading to the formation of continuous network in liquid phase called the gel through gelation of the sol. The precursors used for the process contains metal or metalloid compound surrounded by reactive ligands. The chemistry of sol-gel process is well understood using metal-alkoxide

compounds. The basic metal-alkoxides are alkoxysilane groups: tetraethoxysilane (TEOS) and tetramethoxysilane (TMOS). The sol-gel process involved in the preparation of hybrid di-ureasil can be compared to the sol-gel process of alkoxysilanes namely TEOS. In this section, the chemistry of sol-gel process is explained using the alkoxysilane group (TEOS). The three step reactions involved in the process are: hydrolysis, alcohol condensation and water condensation [23][24].

Hydrolysis reaction:

The reaction (4) shows the hydrolysis reaction which is the first of the three step Sol-Gel process. The group represented **R**, is an alkyl group.

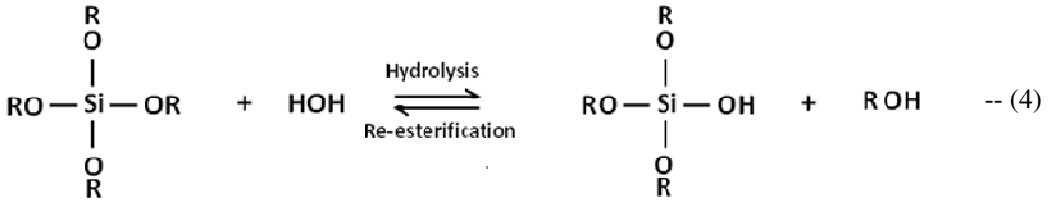

-- (4)

During this reaction the water molecules reacts with the alkoxysilanes and removes the alkoxides group, replacing it with the hydroxyl groups. This leads to the formation of silonal groups (Si-OH) [23] [24].

Condensation reaction:

The next two steps of the process involve water and alcohol condensation, leading to the formation of siloxane bonds (Si-O-Si). The silanol groups formed during the hydrolysis reaction reacts to form these bonds. The condensation starts even before the completion of the hydrolysis reaction in most conditions of the reaction. During the condensation process the Si-O-Si bonds increases leading to bridging and aggregation of the individual molecules in the sol. Gel formation occur once when these aggregates start forming the networks. At the next stage during drying the volatile compounds are removed from the network shrinking the whole system. As shown in the equations excess addition of solvents leads to reverse reactions leading to esterification and de-polymerisation [23][24].

- *Water condensation reaction*

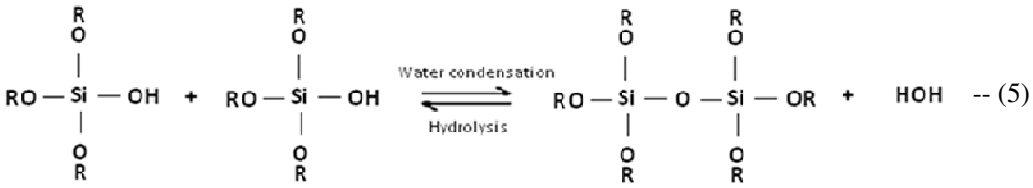

During the water condensation the silanol groups reacts together forming the siloxane bonds and leaving out H_20 as byproduct as shown in reaction (5) [23][24].

- *Alcohol condensation reaction*

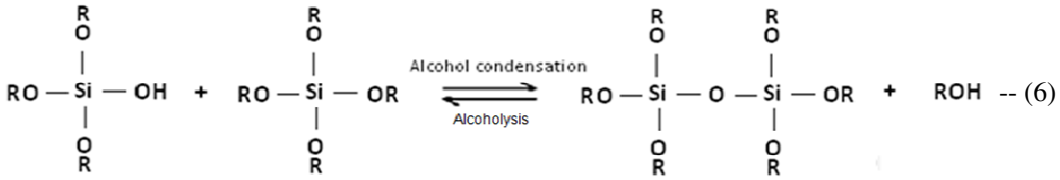

As shown in reaction (6), in an alcohol condensation the silanol groups react with the alkoxysilane groups and form the siloxane bonds producing alcohol as a byproduct. The gelation occurs basically in three steps; polymerization of the monomers to form particles, growth of particles and particle linking to form chains that networks extending throughout the liquid to form gel. The particles size grows in a basic solution in the absence of salts. In a acid solution or in a basic solution with salts present in it, the particles aggregate and form three dimensional networks leading to gelation [23][24].

- *Influence of pH*

The polymerization process is influenced by the pH of the system and is shown in Figure 2-6. The dependence is divided into three pH domains; pH < 2, pH 2-7, pH > 7 [23] [24].
(a) pH 2 being a point of zero charge makes the surface charge to be zero and the electrical mobility of silica particles are zero making it 'isoelectric point'. In the metastable region of pH < 2 the gel times are long. At this range of pH the polymerization is proportional to the concentration of protons in the system.

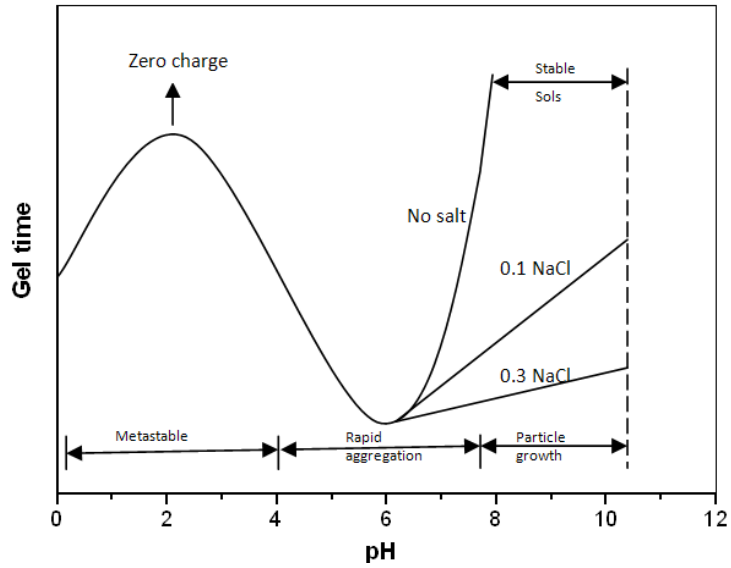

Figure 2-6 pH dependency of the Sol-gel process in aqueous silicates [23].

(b) In the pH range 2 - 7 the condensation rate is proportional to the OH^- concentration.

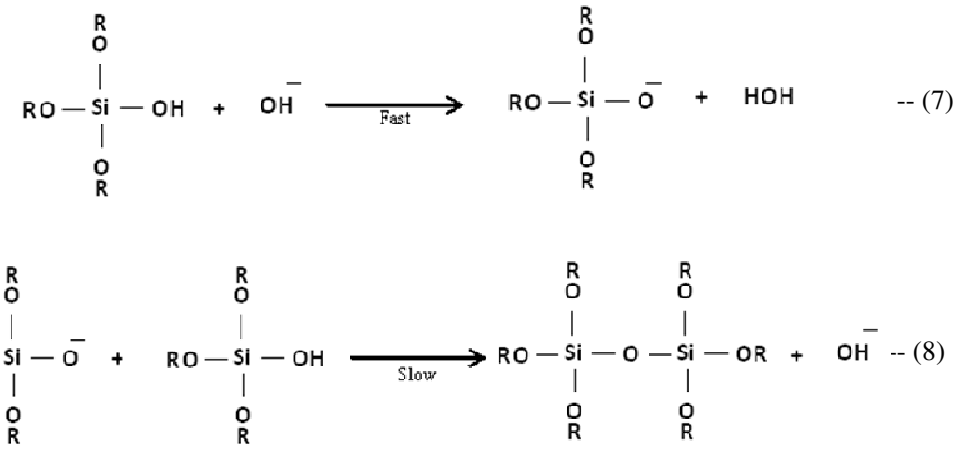

The reaction (7) shows the acidic silanol species being de-protonated by hydroxyl ions. As in reaction (8) condensation takes place between de-protonated silanol species and protonated neutral silanol species, making the dimerisation process slow. But once the dimers form it reacts with monomers to form trimers and the trimers react with monomers to form tetramers. The closeness of chain ends and the depletion of monomers speeds up the cyclization. Further growth occurs by addition of small molecules to bigger species and by aggregation of condensed species to form chains and networks. When the pH is near iso-electric point, growth and aggregation of particles take place together. The solubility of

silica is low at this pH range stopping the particle growth to not more than 2 - 4 nm [23] [24].

(c) At and above pH 7 the solubility of silica and the dissolution rate are maximized. Here the polymerization is same as in equations (7) and (8) but at this range of pH, there is addition of monomers to highly condensed species instead of aggregation. At this range Ostwald ripening takes place where small particles dissolve and re-precipitate to form larger less soluble particles. The particle growth also depends on temperature and the particle size distribution. At higher temperatures silica solubility increases producing larger particles. The absence of salt particles leads to formation of Sol containing large particles and in the presence of salts the gelation is faster [23] [24].

Catalyst effect on the process:

Strength and concentration of the acid or base used as the catalyst for the process influences the reaction as well as the final product resulting from the reaction [23][24].

- *Catalyst influence on Hydrolysis*

In an acid catalyzed hydrolysis reaction, the protonation of alkoxide group occurs rapidly at first. The base catalyzed hydrolysis reaction is slow as compared to acid catalyzed reaction.

- *Catalyst influence on condensation*

In an acid catalyzed condensation reaction, the protonated silanol reacts with neutral species. Since a protonated silanol is more electrophilic, it is susceptible to nucleophilic attack.

As seen in figure 2-7 the silicon oxide networks that result under acid catalyzed reaction are primarily linear or randomly branched polymers which form additional branches leading to gelation.

Figure 2-7 System formed from acid catalysis [24].

A based catalyzed condensation result in highly branched clusters as shown in figure 2-8. These clusters behave as discrete clusters in the system [23][24].

Figure 2-8 System formed from base catalysis [24].

The characteristics and properties of material produced from sol-gel process depend on the various parameters that change the morphology of the network. The parameters having control over the rate of hydrolysis and condensation are: pH, reaction temperature, time of the reaction, reagent concentrations, catalyst nature and concentration, H_2O/Si molar ratio, aging temperature and time, and drying process. The widely used process parameters to control structure and property of the system are the pH, catalyst, temperature and H_2O/Si molar ratio [23][24].

2.5 Spin coating

Spin coating is a technique to deposit thin film layers on flat substrates. The substrate with the solution is spun off at a high speed and a uniform layer is formed on the substrate. The advantages of spin-coating are rapid processing, easy operation and use of small amounts of liquid for large deposition areas. Spin coating device is called as a spin coater. It consists of a high speed motor with a vacuum plate connected to vacuum pump which provides vacuum to hold the substrate. Thin film properties can be tailored by changing the parameters like the rotation speed, viscosity of the sol, acceleration, time and atmosphere. It is then taken for next processing like the heat-treatment to get the final product. Spin coating basically is split into four stages. Depositing the coating solution on the substrate is considered to be the first stage, as illustrated in figure 2-9. It is done either by spraying or pouring the solution through a nozzle. To avoid dust particles and flaws in the solution, sub micron sized filter is used to dispense the solution. The important aspect

to be noted during dispensing is whether we get the total coverage (*i.e.* whether the substrate is completely wet by the solution or not) [25][26].

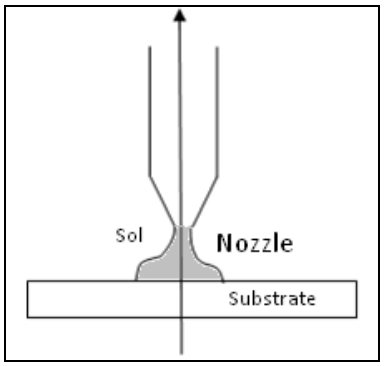

Figure 2-9 Spin coating Stage1.

The second stage involves the substrate rotating at the desired rotation speed, illustrated in figure 2-10.

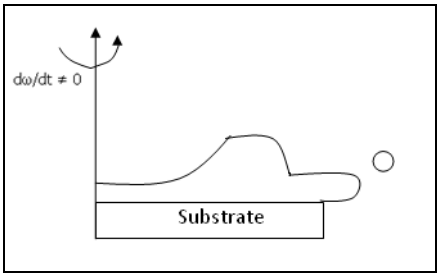

Figure 2-10 Spin coating Stage 2

Fluid expulsion occurs from the surface due to rotational motion. Spiral vortices are formed during this stage, resulting from the inertia exerted by the top fluid layer during the twisting motion of the fluid. At this time the substrate below, rotates faster and at a certain time, fluid becomes thin enough to co-rotate with the wafer [25][26].

In the third stage, at a constant spinning speed, there is a uniform fluid thinning on the substrate due to viscous behavior. Due to outward flow we can notice edge effects of the layer. Such effect causes slight thickness change in the rim of the film. The origin of these edge effects includes surface tension, viscosity, rotation rate, etc. Uniform coating occurs when there is Newtonian viscosity and uniform fluid thickness from the start [25][26].

The fourth stage gives rise to evaporation of the solvent at a constant spinning, as shown in figure 2-11.

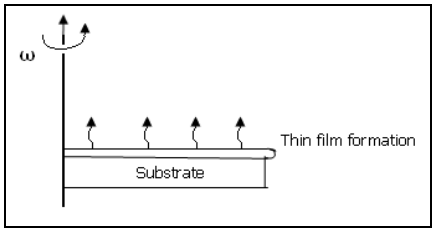

Figure 2-11 Spin coating Stage 3 and Stage 4.

At a certain time, fluid flow stops minimizing the viscosity effect of the net fluid flow. This is the point where the evaporation begins. Evaporation of solvent leads to gel formation as the solution viscosity keeps increasing [25][26].

- *Common defects occurring in a spin coating process*

Comets

When normal flow of the solution on the spinning substrate is hindered by large solid particle, it will lead to formation of comets as seen in the figure 2-12.

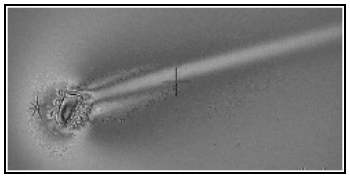

Figure 2-12 Spin coating defect - Comet [25].

Working in cleaner environment and by filtering the coating solutions the formation of comets can be prevented [25].

Striations

Radially oriented lines of thickness variation over the films are said to be striations. The orientations of the variation of thickness normally rely on the direction of major fluid flow. The variations in thickness are usually smooth caused due to surface tension effects resulting from evaporation of solvent. Figure 2-13 shows the surface tension (σ) influence on thickness variation. At higher surface tension the liquid is pulled inwards causing thickness variations [25].

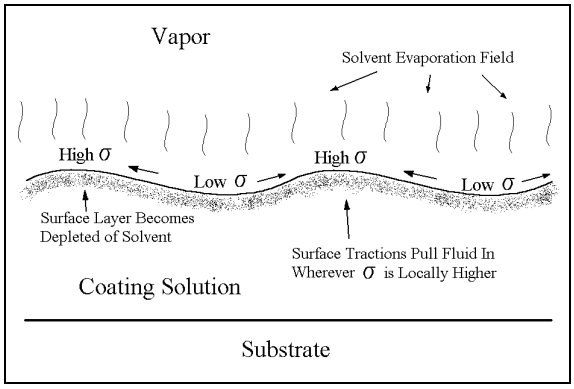

Figure 2-13 Spin coating defect - Formation of striations [25].

Chuck marks

Marks as seen in figure 2-14 are caused by the back side contact of the substrate material with vacuum chuck of the spin coater. It is said that it occurs because of thermal conduction of the substrate (thermal communication between film and vacuum chuck through substrate), since there is no real contact between the film and the vacuum chuck [26].

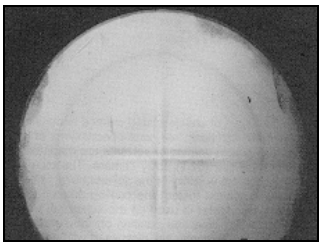

Figure 2-14 Spin coating defect - Chuck mark [25].

Environmental sensitivity

Coating environment influences the quality of sample which may cause roughness, micro-cracking of the coating upon drying, exaggerated striation formation in the coating, etc. For example the humidity around the coating area will have direct effect on the chemistry of the coating solution, which directly will affect the coating quality [25].

Edge effects

The edges of the substrate usually have improper coating. In a circular substrate, due to surface tension, small bead of liquid get attached around the perimeter resulting in thicker

coatings in rim zone. In square and rectangular substrates there exists non-uniformity in coating thickness in the corner areas as seen in figure 2-15 [25].

Figure 2-15 Spin coating defect - Edge effect [25]

2.6 Prism coupler technique

The prism coupler method is used to determine the refractive index and thickness of dielectric thin films as well as metallic films. It only requires the experimental measurement of the incident angle and a software application to compute the refractive index [11][12]. The experimental setup used for the thesis was a homemade system and is described in the experimental section.

In this technique, to obtain the refractive index and thickness of thin films, the thin film must be pressed against the base of a high refractive index prism. The film and the prism base are fixed together with an air gap between them. Light beam from a laser beam source is introduced into the waveguide through the prism. When the phase velocity of the wave in the film equals the phase velocity of the incident light, coupling of light from the prism into the thin film take place. This lead to the excitation of guiding mode into the film with high efficiency and the incident light is confined in the film. Trapping of the light occur due to total internal reflection (TIR), which takes place in waveguides at angles above a critical value. The total internal reflection depends on wave guiding film's refractive index and the refractive indices of mediums surrounding the waveguide [11][12].

- *Coupling phenomena*

Figure-2-16 illustrates the coupling phenomena between a prism and a film. When laser beam strikes through one face of the prism on to the base of the prism, the beam is reflected on to other face of the prism. The overlapping waves of the incident and the reflected beam generate a standing wave. The evanescent field of the standing wave penetrates into the waveguide through the air-gap. At a certain angle of beam incident on base of prism, there occurs phase matching condition that stimulates guiding mode in the

film following which total internal guiding of wave through film take place. Here it is evident that the air gap place important role for coupling to occur. The film must be at a certain distance from the prism base. This is because the waves are decaying waves and guiding cannot be attained if the gap is wider, which will lead to scattering. As well if there isn't any air gap or very low refractive index medium between the prism and the film, there is no formation of evanescent wave and there is no wave coupling into the film. The refractive index of the prism must at least be as high as the effective refractive index of the waveguide to achieve the phase matching condition [27].

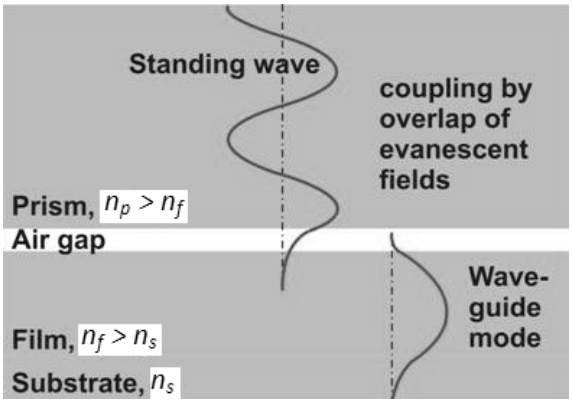

Figure-2-16 Coupling phenomena between the prism and the film [27]

The figure 2-17 depicts a basic arrangement of a prism coupler showing a thin film on a substrate attached to a prism.

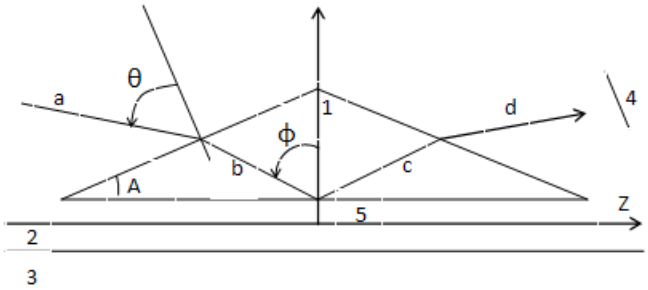

Figure-2-17 Basic setup of a Prism coupler [12]

1 -- Prism with refractive index n_p, 2 -- Thin film with thickness t and index n, 3 -- Substrate with refractive index n_0, 4 -- Photodetector/Screen, 5 -- Air gap with index $n_2 = 1$, θ -- Incident angle at prism base, A -- Base angle of prism, ϕ -- Beam angle formed to the normal at base **a**→incident beam, **b**→beam onto base, **c**→reflected beam from base, **d**→beam to photodetector

The waveguide will have certain number of allowed modes, depending on the thickness and refractive index of the film, at which it can guide the coupled wave from the prism. Varying the incident angle θ of the input beam (a), different modes of the waveguide can be excited. The incident beam (a) is refracted on one face of the prism and it gets diffracted as beam (b) which falls on or near to centre of the prism base. This beam is either coupled on to the thin film or reflected back as beam (c). When there is coupling in the film, the intensity of reflected beam (c) decrease. This variation affects the beam (d) coming out of the prism face. The angle shown by the goniometer is noted for very low intensities of the beam (d), since at these angles the incident wave on the prism base is guided into the film. To correctly detect the variation of beam (d) intensities a photo-detectors are used. The light beam (b) which enters the prism makes an angle ϕ to the normal of the film surface. The angle ϕ governs the phase velocity in the z direction. This angle is calculated from the incident angle θ [11][12].

Equation (9) gives the phase velocity, v_i:

$$v_i = \frac{c}{n_p \sin\phi} \quad \text{-- (9)}$$

where c is speed of light in vacuum, n_p is prism refractive index and ϕ is the angle formed by the beam on the base of the prism with the normal.

The phase velocity of a guided mode on the waveguide is given by:

$$v_m = \frac{c}{N_m} \quad \text{-- (10)}$$

where m is the guiding mode number (m =0,1,2….) and N_m the effective refractive index of the m^{th} mode.

$$N_m = n_p \sin\phi_m \quad \text{-- (11)}$$

The efficient coupling of light into the waveguide occurs when $v_i = v_m$.

Since, the angle ϕ_m cannot be measured directly, relating ϕ_m to θ_m (angle of incidence corresponding to each mode), the effective index can be obtained by:

$$N_m = n_p \sin\left(\frac{\sin^{-1}(\sin\theta_m)}{n_p} + A\right) \quad \text{-- (12)}$$

where A is the base angle of the prism.

The film effective refractive index (n) and the thickness (t) can be found using the following *eigen-value* equation (13) *(where $N_m = N(m,n,t,k,n_s,n_e,\rho)$*

$$\left(\frac{2\pi}{\lambda}\right) t(n^2 - N_m^2)^{1/2} = m\pi + \phi_s + \phi_e \quad (m = 0,1,2 \ldots) \qquad \text{-- (13)}$$

where λ is the wavelength of the light beam in vacuum, $k = 2\pi/\lambda$, ρ -- *TE/TM polarization*

The phase change in the film substrate (ϕ_s) and the phase change in the tip layer, usually air-gap (ϕ_e), are given respectively by, (*here $n_f = n$*)

$$\phi_s = \arctan\left[r_s \left(\frac{N_m^2 - n_s^2}{n_f^2 - N_m^2} \right)^{1/2} \right] \qquad \text{-- (14)}$$

$$\phi_e = \arctan\left| r_e \left(\frac{N_m^2 - n_s^2}{n_f^2 - N_m^2} \right)^{1/2} \right| \qquad \text{-- (15)}$$

where r_s and r_e are constants which depend upon the mode of light beam. For the TE mode both the constants have a unitary value (TE mode was used in this work). For TM mode, the constant values are given by $r_s = \left(\frac{n_f}{n_s}\right)^2$ and $r_e = \left(\frac{n_f}{n_e}\right)^2$ [11][12].

The iteration of the *eigen-value* equation (Equation-13) is done by using a numerical optimization routine providing it with an initial value of the thickness (t) and refractive index (n). For this thesis a MATLAB based software was used to get the refractive indices and thicknesses from the system parameters (refractive index of prism (n_p), refractive index of substrate(n_s), wavelength of light λ and the incident angle θ) [32]. To solve the equation (13) and to get the unknown values, at least two effective refractive indices values are needed, which is possible only when the waveguide supports two modes of the same polarization. From a practical point of view, when the film thickness is high, it supports more number of modes, resulting in more accurate values for the estimation of n and t [11][12].

- *Refractive index and thickness computation*

The experimentally found values which are the incident angles (θ) corresponding to the respective mode numbers (m) along with the constants *(m,n,t,k,n_s,n_e,ρ)* are fed to a software application. At first the observed propagation constants are measured by the software relating the experimental values and constants with the equation (12). Using the dispersion equation (13), which relates the film refractive index and thickness with the constant parameters, the values of unknown n and t are calculated. Before the iteration (to evaluate

the unknowns n and t) to begin, an intial value for n and t is given to the software. If there are two modes say 0 and 1 of the same polarization, the practical effective index values of mode 0 and 1 which are calculated from equation (12) are substituted in equation (13), yielding to two different equations. Relating the two equations and eliminating the k and t value we get an equation which is a function of n^2. By mathematical procedure and iteration of this equation, n value is found and eventually t value is calculated from equation (13) substituting n. When the film supports more number of modes, the self consistency of the measurements and the accuracy of n and t values increase [12]. The fundamental principle of MATLAB developed software used for this thesis to evaluate refractive index and thickness is briefed in the experimental part.

2.7 UV exposure on hybrid materials

Sol-Gel process conventionally depends on heating to bring about crystallization and densification of amorphous gels. To improve the properties of organic-inorganic hybrid materials, changes are to be brought at low temperatures. The UV irradiation is well suited for this purpose, since it leads to direct activation of chemical bonds present in sol or gel at room temperature. Due to the demand of low temperature synthesis routes for the preparation of hybrid material devices, the change in chemical reaction in sols or gels and the modification of gel networks to modify its properties (especially its refractive index), are done using this method. Other advantage is the spatial selectivity which makes UV radiation more advantageous than conventional heating to modify the material properties. During thermal excitation (phonon mode) of UV radiation, local temperature at the surface is increased and during the electronic excitation (photon mode) the organic and inorganic components are excited. UV irradiation is also used for pre-treatment before conventional annealing process of material. This lowers the process temperature improving the film morphology. Patterning of sol-gel films and photolysis reactions of sol/gel can be achieved using UV irradiation. It must be taken in consideration that the photon energy and fluence of the UV radiation influences the sol-gel process. The figure 2-18 shows schematically the effects induced by a UV irradiation on photosensitive material [25].

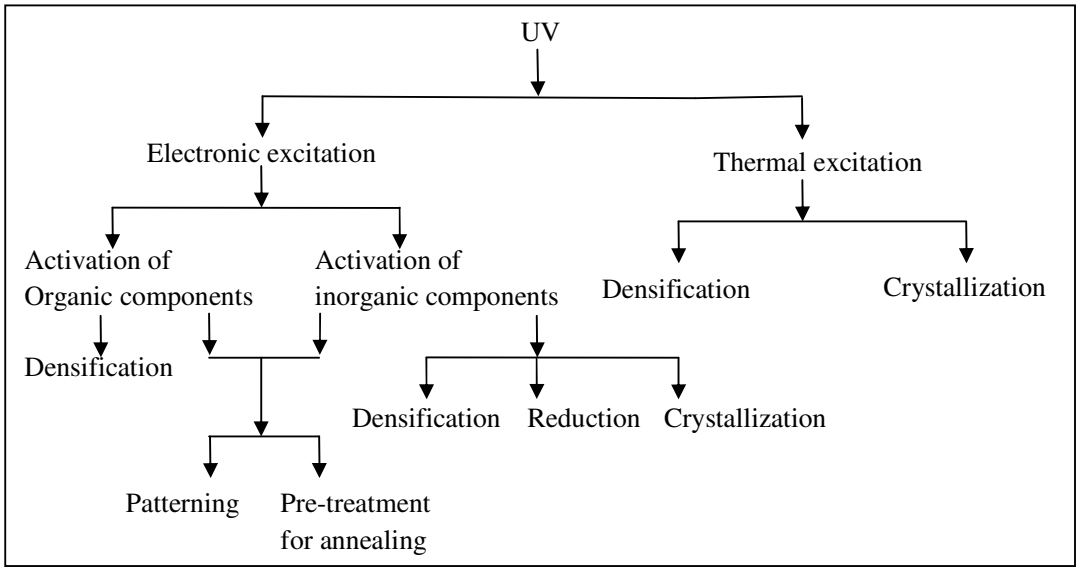

Figure 2-18 Effects induced by UV exposure in photosensitive sol-gel systems.

As shown in figure 2-19 electronic excitation in the organic compounds (metal alkoxides) leads to decomposition of alkoxyl groups.

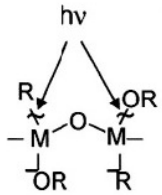

Figure 2-19 Excitation of organic component [25].

The system undergoes a change in the solubility due to photochemical reaction that result from the excitation of organic bonds. The inorganic excitation leads to drastic structural changes due to densification, crystallization and reduction as seen in the figure 2-20.

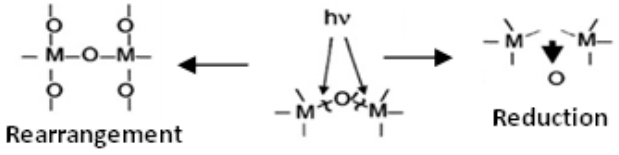

Figure 2-20 Excitation of inorganic component [25].

In this excitation photons with higher energy than the band gap of material, leads to band-to-band excitation causing excitation of electrons through bandgap of oxides and charge transfer from O^{2-} to M^{x+}. The recombination of free electrons and positive holes in the crystal structure deactivates the excited states. In the amorphous structure and at the surface localization of free electrons and holes at disordered sites leads to cleavage of M-O-M bonds. Rearrangement of networks through densification, crystallization and release of oxygen called 'reduction' are caused due to this cleavage. Thermal excitation of the material also occurs especially when using coherent UV source [25]. The development of organic-inorganic hybrid materials with high functionality like direct writing of channels and the possibility of selective excitation of target components make UV irradiation well suited in processing of nano-functional optical components [25].

- *UV absorption and chemical bonding*

The response of hybrid materials to UV radiation is influenced by different kinds of bonding present in organic and inorganic parts of the network. UV-visible absorption spectrometry is based on Beer-Lambert law which says the absorbance is directly proportional to path length of UV-visible beam, concentration of material and molar absorptivity (constant of proportionality) [29]. For easy understanding UV absorption relation with chemical bonding we can relate the types of UV absorption that is present in d-UZ(600). The absorption coefficient values of unexposed samples discussed in the Chapter-4 shows that its value increased with cluster concentration, d-U(600) films having the lowest value. The main form of electronic transitions causing UV absorption can be related to s (σ-zigma), p (π-pi), non-bonding and charge-transfer electrons jumping to its corresponding anti-bonding energy level and other higher levels [29][30]. The pure d-U(600) UV absorption can be related to its Si-O-Si bonding (charge transfer complexes) and the amine (nitrogen containing non-bonding/lone pairs of electron) and carbonyl group (containing C=O π bonding) of the urea group. As the increase of cluster concentration increases absorption and refractive index, discussion of absorption relating to its concentration is more relevant and is briefed in the following.

The functional group (methacrylate) present in the Zr-oxo-cluster containing C=C bonding and the Zr^{4+} along with oxygen which are considered the charge transfer

compounds are the main cause of UV absorption. These are said to cause π - π* electron excitation and charge transfer complexes, contributing to 1000-10000 cm^{-1} and more than 10000 cm^{-1} values of absorption coefficient respectively [29][30]. When the concentration of methacrylate group and Zr-O bonding increases it will also increase the UV absorption of the total system.

- *UV absorption and refractive index*

The refractive index change with respect to UV absorption coefficient can be explained with color centre model called Kramers-Kronig (KK) relationship which relates change in refractive index with absorption behavior. The relationship is cause of photooxidation and sensitization. It gives the direct proportionality of refractive index change to absorption coefficient change.

Kramers-Kronig relation is given by,

$$\Delta n(\lambda') = \frac{1}{2\pi^2}\int_{\lambda 1}^{\lambda 2} \frac{\Delta\alpha(\lambda)}{1 - \lambda^2/\lambda'^2}\, d\lambda \qquad \text{-- (16)}$$

λ1and λ2 are boundaries of the spectral range, λ' is wavelength where refractive index is calculated and Δα is absorption coefficient value [31].

3. EXPERIMENTAL PROCEDURE

3.1 Preparation of di-ureasil Methacrylic acid modified Zirconium oxoclusters

Figure 3-1 shows the flow-diagram for the synthesis of d-UZ(600) thin films. The process of the thin film preparation involves, synthesis of the 'sol' containing methacrylic acid modified Zirconium-oxo-clusters in the precursor (d-UPTES) containing different ratios of the material and its deposition onto substrates using spin coating technique. The film deposition is followed by heat treatment to evaporate the residual solvents [18].

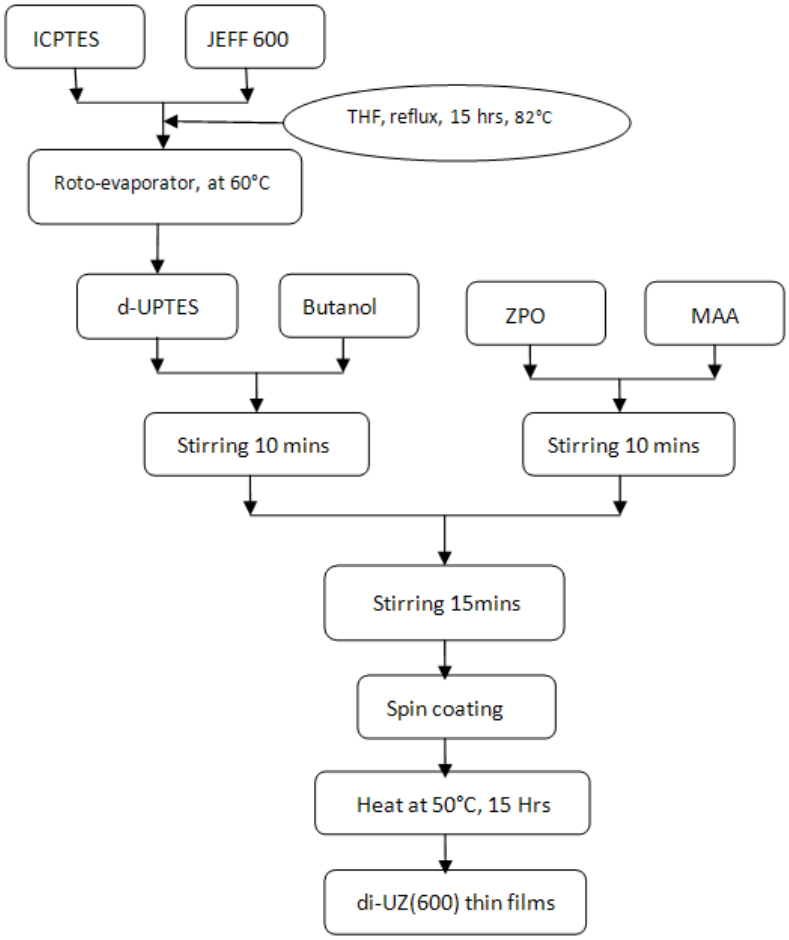

Figure 3-1 Flow chart of synthesis of the thin films through sol-gel process.

- *Synthesis of di-ureasil precursor (d-UPTES(600))*

The organic – inorganic hybrid material named d-U(600) is made of polyether containing siloxanes at their ends connected through urea functionalities. This compound is

synthesized mixing ICPTES (Sigma Aldrich, (3-isocyanatopropyl)triethoxysilane, MW 247.37 g/mol, 95%) and Jeffamine ED600 (Fluka, Sigma Aldrich, 0,0`-Bis-(2-aminopropyl) polypropylene glycol-block-polyethylene glycol-block-polypropylene glycol 500, MW – 600 g/mol) in molar ratio 2:1. The terminal amine groups of Jeffamine ED-600 and the isocyanate group of ICPTES form the urea linkages. The resulting mixture is then stirred for 10 mins adding Tetrahydrofuran - (THF, Riedel-de Haën, Honeywell, 2,6-di-tert.-butyl-4methylphenol, MW – 72.11 g/mol, 99%). THF was taken in ratio with respect to silicon, 1:3 (Si:THF). During stirring this mixture, temperature was maintained at 82°C and stirring was done for 15 hrs and THF was retained by reflux method. The THF solvent was removed to form pure d-U(600) by using a rotoevaporator. In the rotoevaporator setup the mixture was kept in a water-bath and stirred constantly at 60°C to remove the solvent to get the 'di-ureasil' [18].

- *Preparation of the precursor MAA-modified $Zr(OPr^n)_4$*

The precursor used for preparation of d-UZ(600) was formed mixing Zirconium (IV) Propoxide ($Zr(OPr^n)_4$) (Sigma Aldrich, 70wt% solution in 1-propanol) and Methacrylic acid (MAA) (Sigma Aldrich, (CH_2=C(CH_3)C(=O)OH), 99%) at room temperature using the stirrer for 10 mins. d-UPTES sols containing various concentrations of MAA modified Zr-oxocluster were prepared. This was achieved by varying precursor concentrations. Molar percentage concentration of Zr in $Zr(OPr^n)_4$ and Si in UPTES were used as reference. The ratios prepared were Si:Zr - 80:20, 60:40, 40:60. MAA concentration was changed in ratio with respect to Zr. The ratios used were Zr:MAA - 10:1, 5:1, 2:1, 1.5:1, 1:5, 1:10. For transferring solutions into beakers, micropipettes those having volume range of 100 - 1000 µl and 20 - 200 µl manufactured by SOCOREX were used. Care is taken when transferring $Zr(OPr^n)_4$, since it readily reacts with moisture and hydrolyze and condensate (precipitate), forming white powders [18].

- *Synthesis of Di-ureasil – Zr-OMc hybrids*

The d-UPTES(600) precursor was mixed with Butanol (BtOH - Sigma Aldrich, 1 – butanol, 99.9%, MW 74.12 g/mol) in ratio of Si:BtOH 1:2. The d-UPTES precursor was

measured using PRECISA XB 2200C (Max.220g Min 0.5g) and RADWAG AS 220/C/2 (Max 220g Min 10mg) instruments. Since one UPTES molecule contains 2 Silicon atoms, volume of BtOH is prepared accordingly. The two compounds necessary for the synthesis of di-ureasil – Zr-OMc hybrid are stirred for 10 mins. This suspension is mixed to the MAA-modified $Zr(OPr^n)_4$ and stirred for 15 mins to get the sol containing MAA-modified $Zr(OPr^n)_4$ particles in d-UPTES. All the reactions were carried out at room temperature [18].

3.2 Thin film processing

The table 3-1 shows the thin film parameters which were processed and used for this study.

Table 3-1 Studied sample details (Sample ID, Si:Zr:MAA ratio, MAA molar concentration, No. of samples prepared, and details of experiments done with sample)

Sample id	Si(UPTES): Zr(ZPO)	MAA Conc.(M)	No. of samples used	UV Exposure for various times*	Prism coupler measurement	Absorption Spectrum*
W0	100:0	0	8	✓	✓	✓
W1	80:20 Diluted System	0.15	8	✓	✓	✓
W2		0.19	8	✓	✓	-
W3		1.20	8	✓	✓	✓
W4		2.30	8	✓	✓	✓
W5	60:40 Intermediate System	0.40	8	✓	✓	✓
W6		2.40	8	✓	✓	✓
W7		4.05	8	✓	✓	✓
W8	40:60 Concentrated System	0.70	8	✓	-	✓
W9		3.70	8	✓	✓	✓
W10		5.60	8	✓	-	✓

Exposure times* - 4, 6, 8, 10, 12, 16, 32 hours

Absorption Spectrum* - carried out using UV/VIS spectrometer Jasco instrument Model V-560

The prepared 'sol' was deposited onto boron silicate (SCHOTT Nexterion Glass B 25x75.6x1mm) substrate and coated by spin-coating method to get the thin films. The Boron silicate substrates were cleaned with acetone and ethanol. Micropipettes with plastic disposable tips were used to spread 700 ml of sol on the substrate for each sample. For every spreading new tip was used. Spin coating was carried out using the Spin 150, APT GmBH machine which uses an external vacuum pump to provide vacuum to hold the substrates. Spin coating was done in one step at 1000rpm for all concentrations and the films were spun for 60 seconds. The acceleration used for spin coating was 1000 rpm/s. After thin film formation on the substrates, the films were put to heat treatment in the oven (VACUCELL MMM Medcenter Manufacturer) at 50°C for complete evaporation of the solvent during 15 hrs. Ten films were prepared for each concentration. Since the samples containing higher concentration of Zirconium lead to formation of precipitates (Zr:MAA ratios of 10:1, 5:1, 2:1 (2:1 didn't show precipitation only for samples having Si:Zr-80:20)), they are not good for use as waveguides and hence were not included for the study. For easy use in further discussions, the films are named in W series.

3.3 UV irradiation

For the UV irradiance of the samples, homemade UV chamber containing four Philips TUV PL-L Hg lamps was used. Figure 3-2 shows the emission spectrum of the lamps. The total power emitted by the four lamps is 50 mW, measured with a power meter containing a sensor with a diameter of 17.8 mm.

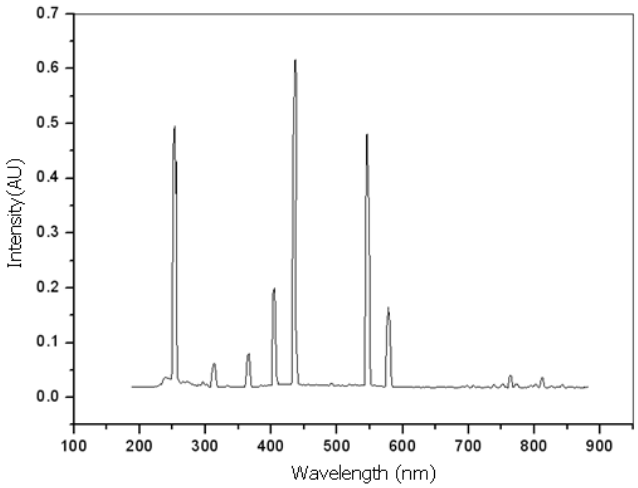

Figure 3-2 UV source emission spectra (PhilipsTUV PL-L Hg lamps, Total Power-50mW).

The wavelength at 255 nm contibutes to 36% of the total emission energy. The measured irradiance (I) value for 255 nm wavelength is 7.263 mW/cm^2. The samples were then exposed to UV irradiation for 4, 6, 8, 10, 12, 16 and 32 hrs (for every exposure unexposed samples were used *i.e* new samples).

$$\text{Energy density } (E) = 26.05 \times \text{time (hours) J/cm}^2 \quad \text{-- (17)}$$

3.4 Prism coupler measurement of refractive index and thickness

The prism coupler experiments to find the refractive indices and the thicknesses of the thin films were done using a homemade setup mounted on an optical bench. Prism coupler measurements of the films were done at three different locations for each film (*i.e* three different readings of mode angles at three locations) and average of the three evaluated refractive index values were considered for the study. Figure 3-3 shows the schematic of the prism coupler setup along with the specifications of the instruments used.

A green laser (L1 - 532.0 nm) and a red laser (L2 - 636.9 nm) source were used for refractive index measurements. Refractive index at two different wavelengths helps in getting required refractive index for a specified application. For example, if we need to attain film refractive index of 1.5 for application in an optical integrated circuit operating at red wavelength, we can choose the best composition of material and necessary UV energy from the graph corresponding to the refractive index trend at 636.9 nm wavelength. The measurement at two wavelengths also gives an idea of the dispersion of refractive index of different samples with respect to the wavelengths. These laser sources are powered by a homemade power source (PS), specifically designed for the input power requirements of the lasers. The prism (P) is mounted on a rotary stage (RS) which is attached to the planar waveguide thin film (F) using a screw (S2). The screw (S1) is used to rotate the stage, which is connected to a digital read out (DRO) unit to measure the incidence angle. The dichroic thin film filter (DF) is transparent to 532.0 nm wavelength and it reflects 636.9 nm wavelengths. The beam coming out from the other face of the dichroic film is reflected by a reflecting mirror (RF) on to the face of the prism. The reflected beam from the prism film interface falls on a photo-detector (PD) connected to a homemade power meter (PM) from which the intensity variation was read.

The first step of the experiment involves fixing the film to the prism base. Care is taken to give the correct pressure when fixing the film using the screw (S2), since it might

damage the film or even crack the prism. Pressure is maintained in such a way that there is an air gap between the prism base and the film.

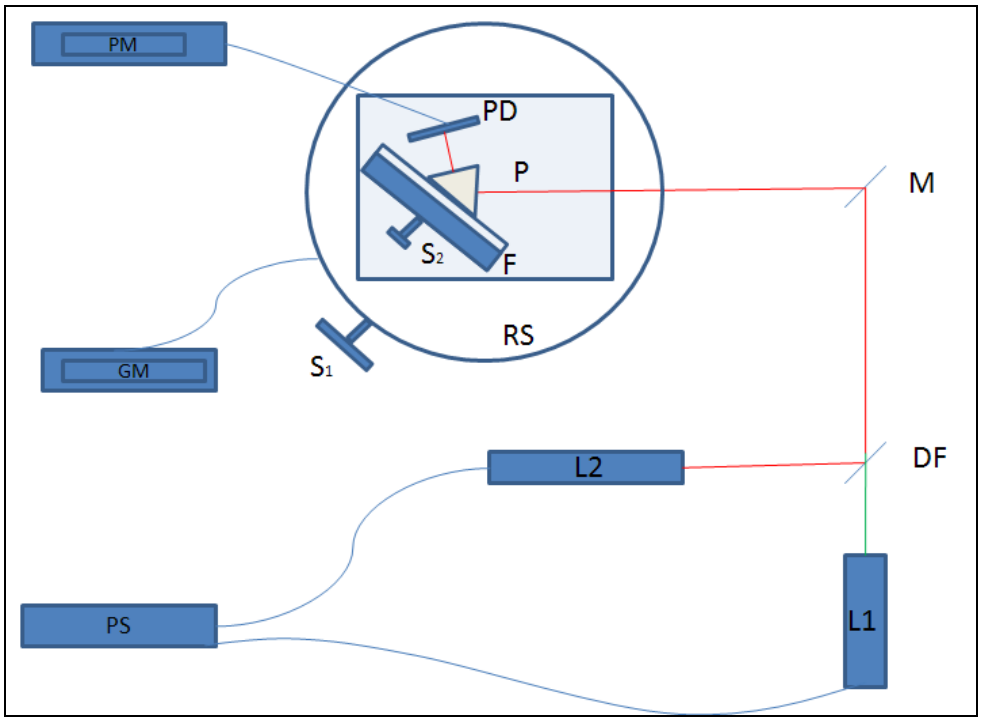

Specifications of the instruments

L1 – Green laser – Roithner Lasertechnik GmbH Model - RLDD532-3-3, Wavelength – 532.0 nm, Power – 3 mW, Beam diameter – 16x60 mm, Beam variance – 0.5 mrad

L2 – Red laser – StockerYale inc., Model – SNF-XXX-635-5, Wavelength – 636.9 nm, Power – 3.57 mW, Current – 56 mA, Adjustable beam diameter

RS - Manual Rotary stage – Model – RT-5DR – Newmark Systems Inc. Powered by 12V power adapter Rotation angle measured by a digital read out (DRO) unit - resolution 9 arcsec, travel - 360° continuous

PD - Photodetector – Model - FDS1010 - THORLABS - Si photodiode, 40 ns rise time, 10 mm x 10 mm active area, 400 - 1100 nm, Responsivity - 0.2 A/W for 532.0nm and 0.35 A/W for 636.9 nm

P - Prism - 10 mm, NT45-949 SFL11 Micro Right Angle Prism, 10 mm on two sides and 14 mm on one side, refractive index - 1.79482 @ 532.0 nm and 1.77812 @ 636.9 nm

DF - Dichroic filter – 580FD70-25 – Andovser Corporation, Substrate material – soda lime glass Circle filter – dia – 25mm, Works in visible wavelength region, Transparent to 532.0 nm and reflective to 636.9 nm wavelength beams

M - Reflecting Mirror – Model PF10-03-G01 - THORLABS - Ø1" (25.4 mm) protected aluminum mirror, substrate material – silica, Reflectivity RAVG >90% from 400 nm to 10.0 µm

PM - Homemade power meter

PS - Homemade power source for the LASERS

Figure 3-3 Prism coupler experimental setup.

To measure the incident angle of the light beam, the beam is made to fall on a side of the prism. Before reaching the prism the beam passes from the laser source through a dichroic filter and is reflected by a mirror. The dichroic filter is used to reflect red laser beam (636.9 nm) and transmit green laser beam (532.0 nm). This is required to keep the setup in the same position unchanged and to keep the axis of the beam at the same spot. The mirror has XY adjustable screws to control the position of the beam (also helps in finding various modes as we can control intensity of the guided beam in the waveguide). The beam is positioned at the centre of the mirror and it is reflected onto the prism face. Rotating the stage at a certain angle, in clockwise direction, we can see the intensity of the substrate guiding mode increasing. When we rotate the stage anticlockwise we can find the modes after the guiding fade away in the substrate. The stage is then rotated clockwise until the prism reflects the beam back on the centre point of the reflecting mirror, at this point the incident angle is perpendicular to the base of the prism and the DRO is set to zero. Now the screw is rotated clockwise and when the power meter deflects to minimum intensity the reading on the DRO is noted down. The readings are tabulated in descending order of the angles in degrees. The maximum value corresponds to mode 0, the second maximum to mode 1 and so on.

Figure 3-4 shows the Prism coupler GUI window image where the parameters are entered in order to get the refractive index and thickness of the respective film. The previously developed prism coupler GUI software application based on MATLAB was used to find the refractive index and the thickness of the films. The measured angles, with respect to each mode, were fed into the software application along with other parameters which are the polarization of the laser beam (L1, L2 are TE mode lasers), the wavelength of the laser source (L1 - 532.0 nm, L2 - 636.9 nm), the refractive index of the substrate (1.474 at 532.0 nm and 1.470 at 636.9 nm), the refractive index of the prism (1.7948 at 532.0 nm and 1.7781 at 636.9 nm), the prism base angle (45°), the initial values for the refractive index and thickness (necessary for the software to use in minimization process) and the maximum number of iterations.

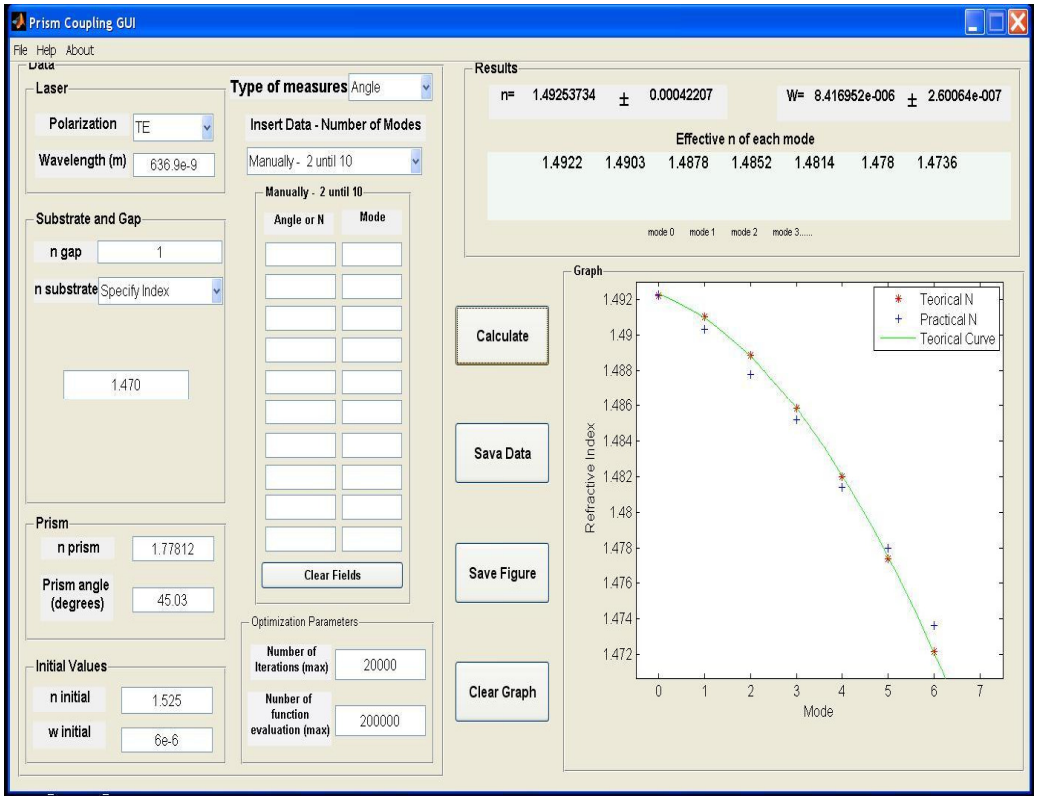

Figure 3-4 Image showing the Prism coupler GUI application interface window

- *Basic principle of refractive index and thickness computation by this software*

The equation (13) is equated to error and the equation is used to find the film thickness and refractive index values along with theoretical effective index of each mode. The equation (13) here takes shape as the following,

$$\left(\frac{2\pi}{\lambda}\right) t\left(n^2 - N_m^2\right)^{1/2} - \left(m\pi + \phi_s + \phi_e\right) = error \qquad \text{-- (18)}$$

Nelder-Mead minimization simplex algorithm is used for the error minimization function [32]. At first the minimization iteration is done by changing the n and t values with the constant practical effective index value until the error is minimum. This is done for effective index of all modes of film. By this we get the film refractive index and thickness values. In the next step the values of theoretical effective indices are achieved by using the measured refractive and thickness values and varying effective index values (N_m) until equation error reaches a minimum. From the theoretical and practical effective refractive indices values the error for refractive index and thickness is given as in the following equation (18).

The home made prism coupler setup has few limitations. (1) The optical power of green laser source is lower than the optical power of red laser source, and the sensitivity of photo-detector is lower for green laser beam as compared to red laser beam. Therefore measurements with red laser are more accurate than the ones made with the green laser. (2) A common disadvantage and limitation to use prism coupler technique is the interaction with the sample on to base of the prism. When this is done, it might lead to a change in the thickness of the film at the point of contact and it leads to changes in the thickness measurement. (3) The error value measured by the software considers only the goniometer error, considering the error calculated from the theoretical and practical effective indices values derived for the refractive index profiling by the software. This error is calculated by,

$$RI_e = STD\ (RI_{te} - RI_{ee}) \quad \text{-- (19)}$$

where, RI_e - refractive index error, RI_{te} - theoretical effective index, RI_{me} - experimental effective index, *STD* - standard deviation function

The error calculation does not consider other error contributing factors. This includes the laser source wavelength, the error to find the maximum intensity of the mode angles (error involved in detector and power meter or visual), and the error involved in the prism refractive index and geometry. Stress effects must also be taken into consideration because the stress applied on the soft thin film will change the film thickness as well the refractive index considerably. The stress effect on refractive index variation is given by Neumann-Maxwell equation. The thickness variations and error relating to thickness depend on many criteria. The film surface and thickness normally vary because of spin coating defects such as striations, edge effects, and dust particles/coating environment. As the prism coupler experiment is a contact technique and organic-inorganic hybrid thin films are flexible and soft, there is higher error involved on thickness measurement, as pressing against the film on prism will affect the thickness measurement. Thickness of the films can be varied using spin coating parameters such as spin speed, acceleration, etc. Also the viscosities of the sol, temperature, UV energy which result in changes such as polymerization, densification, the rate of solvent evaporation directly influence the thickness of the films. The thickness also depends on the cluster concentration which is briefly described in the results and discussion section along with the values of thicknesses measured for the unexposed thin film samples.

4. RESULTS AND DISCUSSION

4.1 Sample quality

The influence of Zr and MAA concentrations on the sample quality was noted during the preparation and during the measurement of refractive index of the films. It was found that for very high Zr concentrations the sample quality was not good. At low Zr concentrations, the films were lacking uniformity. This can be correlated to the work of Xiao Zhang et al [33], in which the study on Zr concentration in a different hybrid host showed that, at lower Zr concentrations the films lacked uniformity. Inability for light guiding was observed in samples containing ZPO along with less amount of MAA and samples with higher cluster concentration. There were formations of white precipitates on the films with very low MAA concentrations. This occurs due to the fact that ZPO has a tendency of reacting readily with moisture in atmosphere to formation oxides leading to precipitation and at low presence of methacrylic acid; the stability of Zirconium decreases. According to Ulrich Schubert [19], the ratio of Zr to MAA must be at least 1:2 for a complete reaction to take place, leading to better formation of clusters. The precipitation was noticed during preparation of samples containing Zr and MAA in ratios 5:1 and 10:1. So it's difficult to make samples containing very low percentage of methacrylic acid with respect to ZPO. But in some systems precipitation was avoided even at very low MAA concentration with respect to ZPO. Samples of d-U(600) and ZPO in ratio 80:20, with very low methacrylic acid (ZPO:MAA - 2:1) showed considerable optical transparency. This was achieved only after leaving the sol prepared at this precursor ratio to react for about 16 hours before using it for film preparation by spin coating. The precipitates disappeared after leaving it to react for a long period and thin films made of it supported wave-guiding. Here it is seen that stable clusters are formed at certain lower MAA concentration with respect to ZPO content which was not expected. This nature of cluster formation at very low MAA concentration was noticed only with diluted samples (*i.e*. samples with 80:20(Si:Zr)) samples and was not detected for 60:40(Si:Zr), 40:60(Si:Zr) where ZPO concentrations are high.

The three different systems (diluted - 80:20(Si:Zr), intermediate 60:40(Si:Zr), concentrated 40:60(Si:Zr)) showed varying guiding property. The diluted and intermediate system samples were transparent while the concentrated system was translucent. The

diluted system showed broadening of the light beam compared to beam that propagated through intermediate system in which the beam guiding was normal. The concentrated system showed higher scattering (no beam line was noticed in the film). In this system light was completely scattered, illuminating the entire film. Better guiding was noticed only for the intermediate system. This shows the concentration effect on the guiding properties of the samples. This also had an effect on the measurement of refractive index, as angle measurement in the experiment involves beam intensity variation according to different guiding modes. For concentrated systems, it was not easy to find the guiding modes and for many samples no guiding was noticed. Also for diluted system samples which have low variation in the refractive index (for varying MAA as well under different UV exposure), the prism coupler limitations reduce the refractive index measurement resolution. It was easy to measure intermediate system's refractive index.

The films changed its color on UV exposure as well as aging (color change - clear to yellowish hue). Darkening in films containing metallic substance usually occur due to the metallic substance in the system as mentioned by Deki et al [34]. In their work, they have studied films made of SiO_2-TiO_2 composites containing Au nanoparticles. Au metal particles were the cause of film color changes. Also reduction causes formation of metal particles [25]. When bond cleavage occurs between metal and oxygen atoms, mobile oxygen atoms are formed. These oxygen atoms escape in porous gel films, leaving metal particles [25]. This behavior is normally detected in sol-gel films exposed to UV. In d-UZ(600) systems, the transparency diminishing behavior and color change was noticed even after some days of UV exposure, showing occurrence of change in the system on exposure to environment and aging. From this we can deduce that degradation or color change of films may occur because of Zr particle formation in the system. Decomposition of the urea group in d-U(600) molecules is basically suspected to cause the yellowish hue of film on aging.

- *Thickness variation of the samples*

Table 4-1 gives the thickness values of the unexposed thin film samples. Previous study on films containing Zirconium clusters in a different hybrid material host showed that increase in the Zirconium content leads to decrease in the film thickness [33]. The

increase in Zr concentration in d-UPTES host material (*i.e.* the d-UZ(600) system) also showed the same behavior for the film thickness changes. From the tabulated values it is evident that, increase in MAA concentration reduces the value of the thickness of the thin films.

Table 4-1Thickness values of unexposed thin film samples

Si (UPTES):Zr (ZPO)	Zr:MAA	MAA Concentration (M)	Film thickness (10^{-6} m)			
			@ 532.0 nm		@ 636.9 nm	
			t	Error	t	Error
100:0	0:0	0	11.4	0.5	11.6	0.5
80:20 Diluted System	2:1	0.15	6.6	0.4	7.1	0.5
	1.5:1	0.19	9.1	0.4	9.1	0.2
	1:5	1.20	8.9	0.1	6.2	0.1
	1:10	2.30	6.0	0.3	6.1	0.7
60:40 Intermediate System	1.5:1	0.40	8.4	0.2	7.6	0.1
	1:5	2.40	5.4	0.2	5.1	0.1
	1:10	4.05	4.7	0.2	4.1	0.2
40:60 Concentrated System	1.5:1	0.70	7.3	0.7	5.6	0.2
	1:5	3.70	4.8	0.1	5.4	0.09
	1:10	5.60	2.4	0.5	3.4	0.1

4.2 Refractive index evolution with change in concentration

The refractive indices for all the unexposed films are tabulated in table 4-2. The maximum index value attained was for the sample W8, 1.5411 ± 0.0012 at 532.0 nm and 1.5321 ± 0.0010 at 636.9 nm. It shows that ZPO plays vital role in refractive index increase. There is less influence of MAA on refractive index change without exposure to UV. This can be seen from the refractive index values of unexposed samples of W8 and W10 where, n (W8) > n (W10).

Table 4-2 Refractive index values (Unexposed samples).

Sample id	Si(UPTES): Zr(ZPO)	MAA Conc.(M)	Refractive index(n) @532.0nm	Refractive index(n) @636.9nm
W0	100:0	0	1.4915 ± 0.0005	1.4860 ± 0.0006
W1	80:20 **Diluted System**	0.15	1.4984 ± 0.0013	1.4858 ± 0.0014
W2		0.19	1.5000 ± 0.0006	1.4929 ± 0.0004
W3		1.20	1.5049 ± 0.0002	1.4940 ± 0.0005
W4		2.30	1.5013 ± 0.0002	1.4937 ± 0.0002
W5	60:40 **Intermediate System**	0.40	1.5043 ± 0.0004	1.4980 ± 0.0002
W6		2.40	1.5163 ± 0.0007	1.5079 ± 0.0006
W7		4.05	1.5205 ± 0.0009	1.5126 ± 0.0017
W8	40:60 **Concentrated System**	0.70	1.5411 ± 0.0012	1.5321 ± 0.0010
W9		3.70	1.5340 ± 0.0007	1.5277 ± 0.0002
W10		5.60	1.5384 ± 0.0006	1.5282 ± 0.0007

The minimum refractive index value was found for the sample containing pure di-ureasil (without presence of methacrylic modified ZPO clusters), 1.4915 ± 0.0005 at 532.0 nm and 1.4860 ± 0.0006 at 636.9 nm. By changing the ZPO concentration the range of refractive index change obtained are 0.0496 and 0.0461 at 532.0 nm and 636.9 nm, respectively. The influence of Zr concentration and MAA concentration are discussed separately in the following. Figures 4-1 and 4-2 show the 3-D plot of Zr and MAA acid concentration influence on the refractive index. It clearly shows that increase in cluster concentration will increase the refractive index values.

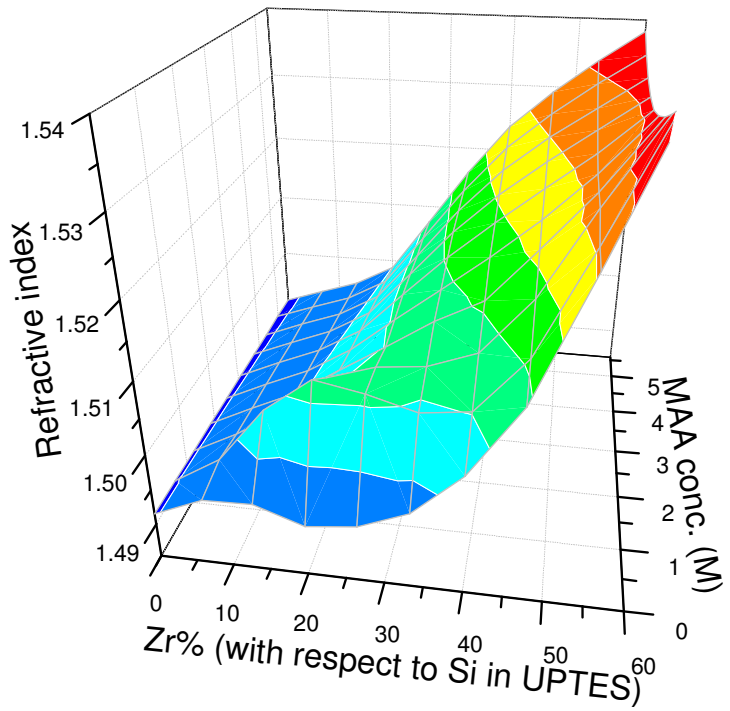

Figure 4-1 *3-D plot* Refractive index as function of Zr and MAA concentration at 532.0 nm

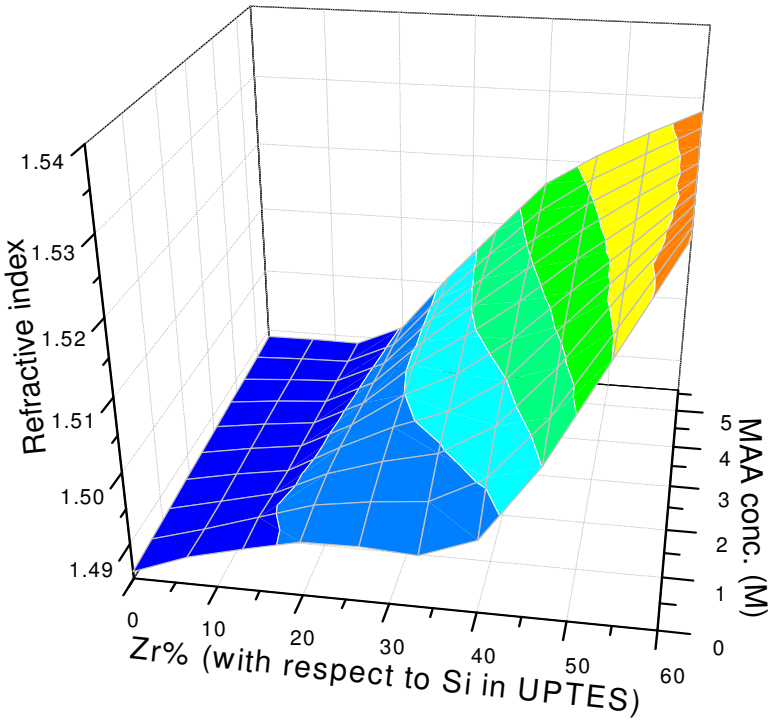

Figure 4-2 *3-D plot* Refractive index as function of Zr and MAA concentration at 636.9 nm

Influence of Zr concentration:

Figure 4-3 illustrates the effect of Zirconium concentration on refractive index change of the samples.

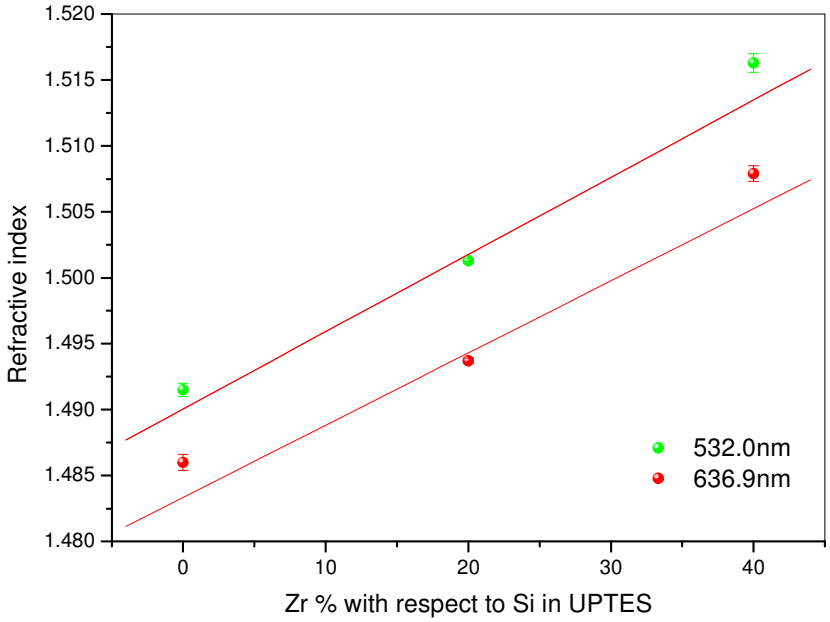

Figure 4-3 Refractive index as function of Zr concentration for unexposed films
The lines are linear fittings.

The trend shows linear increase in the refractive index value as function of the Zr concentration. The increase in refractive index observed in this work shows the same behavior as that observed by various authors for different organic–inorganic hosts prepared for optical applications [33][35][36]. Until a concentration of 40% of ZPO in 60% UPTES saturation for refractive index variation was not observed. Addition of Zirconium has the advantage of giving higher refractive index value for films but at higher concentrations the optical quality of films is compromised and they are not suitable for photonic application.

Table 4-3 shows the linear fit values of the refractive index change as a function of Zr concentration. The lowest value of refractive index in the graph (figure 4-3) is for the thin films having 0% Zr (*i.e.* thin films of pure d-U(600)). The diluted (20%) and intermediate (40%) thin film systems contain almost equivalent concentrations of MAA (*i.e.* 2.3M and 2.4M of MAA respectively). So it can be said that the linear fit corresponds to the ZPO concentration increase with a constant concentration of MAA of about 2.3 or 2.4M.

Table 4-3 Refractive index as function Zr concentration
(Linear fit [$n(t) = n_o + \Delta n \times t$])

λ (nm)	n_0	Error (n_0)	Δn (hrs^{-1})	Error (Δn) (hrs^{-1})	Correlation coefficient
532.0 nm	1.4900	0.0004	0.00058	0.00002	0.9819
636.9 nm	1.4833	0.0004	0.00054	0.00002	0.9658

- *Influence of MAA concentration:*

Figures 4-4, 4-5, and 4-6 depict the influence of methacrylic acid on refractive index for unexposed samples. Refractive index change influenced by MAA variation was noted. For all the three systems, the change in the refractive index is not significant as compared to refractive index change with increasing Zr concentration. For the diluted and highly concentrated system a negligible variation of refractive index was observed, which might be due to very small variation in refractive index or measurement limitation. As well at very low ZPO concentration, there is no uniformity in the films. There is moderate variation in refractive index on changing the concentration of MAA which was noticed for intermediate system.

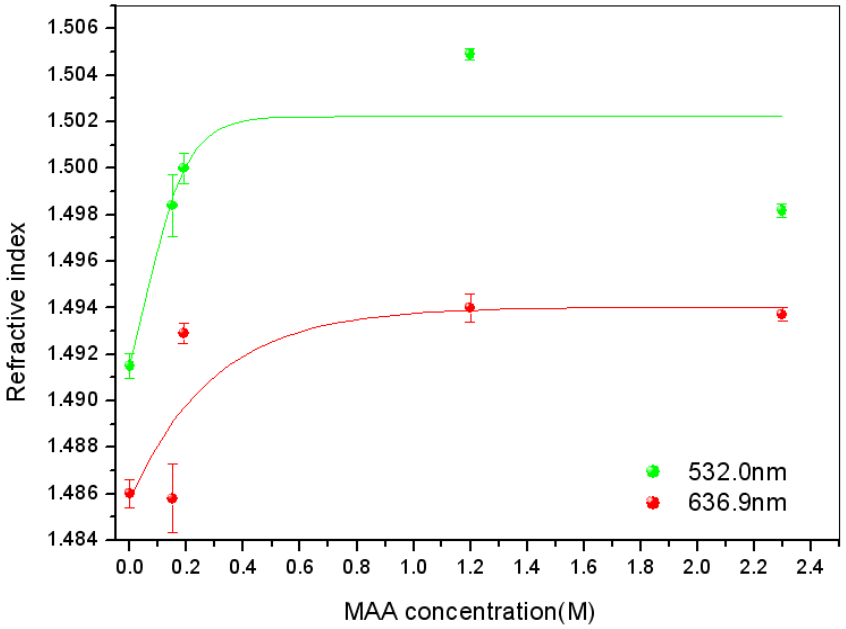

Figure 4-4 Refractive index as function of MAA concentration for 80:20(Si:Zr) unexposed samples. Splines are guides for eyes.

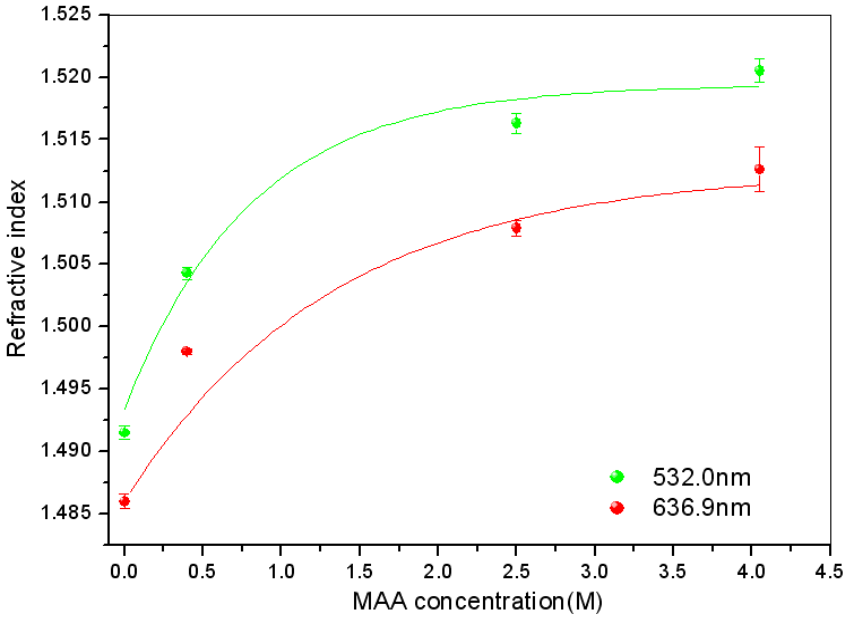

Figure 4-5 Refractive index as function of MAA concentration for 60:40(Si:Zr) unexposed samples. Splines are guides for eyes.

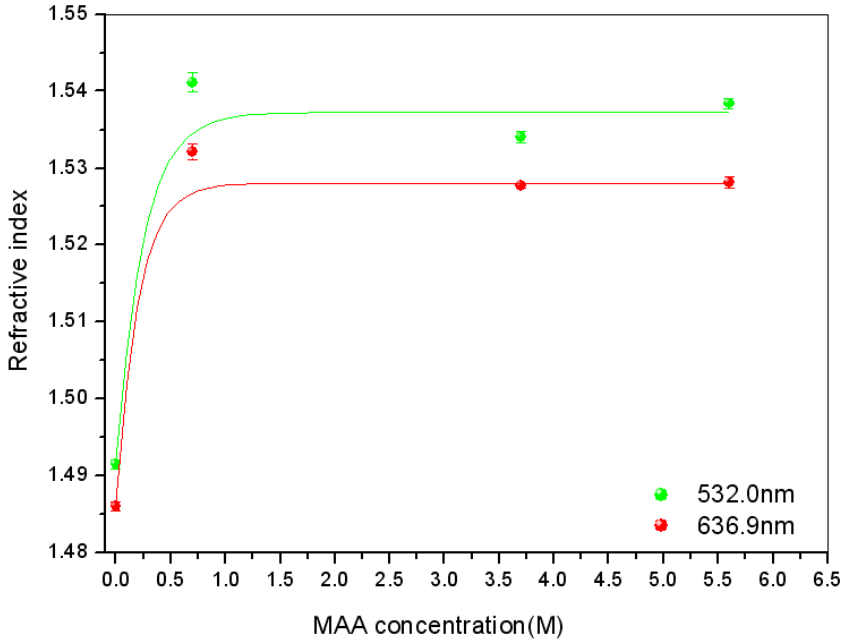

Figure 4-6 Refractive index as function of MAA concentration for 40:60(Si:Zr) unexposed samples. Splines are guides for eyes.

- *Influence of cluster concentration*

Variation in the ratio of ZPO and MAA concentration changes the cluster size, shape and concentration in the system. The changes influence the material refractive index, this can be related to the study on the chemical reaction of the Zr-oxo-cluster formation reported by Ulrich Schubert et al [20]. The properties of hybrid material depend upon the cluster proportion, the kind of cluster, the ratio of functional and non-functional capping ligands, and the polymerization conditions [20]. Thus the refractive index variation of the d-UZ(600) films depend on the Zirconium oxo-clusters, present in the d-UPTES precursor. At lower MAA concentration there is high probability of $Zr_6O_4(OH)_4(OMc)_{12}$ chains formation. As the MAA concentration increase, it is probable that the $Zr_4O_2(OMc)_{12}$ chains are in higher concentration. The concentration of Zr has an effect in the polymerization length of the methacrylate, since it is found that polymerization is influenced by Zirconium dioxide present in the hybrid system [37]. As stated before for a complete polymerization, the Zr and MAA ratio must be 1:2. For lower content of MAA, ZPO without any methacrylate cappings occur in the system and for excess MAA there is presence of monomers MAA or formation of higher amount of $Zr_4O_2(OMc)_{12}$ clusters. These also have an effect on the change in refractive index for samples having Zr content in 20% and 60%.

4.3 Refractive index changes with respect to UV irradiation

- *UV exposure effect on d-U(600) (0% Zirconium & 0% MAA)*

Figure 4-7 shows the refractive index behavior of pure di-ureasil films on exposure to UV irradiation. The different UV exposure times until 32 Hrs, did not show a considerable change in the refractive index of the films. The reason for this behavior is that there are no photo-polymerizable polymers in the system [4]. The sample refractive index shows small variations that can be related to low film quality and the presence of impurities. Therefore ‘di-ureasil’ in pure form cannot be used for fabricating channel waveguides, optical filters, and gratings by UV exposition without addition of photopolymerisable compound.

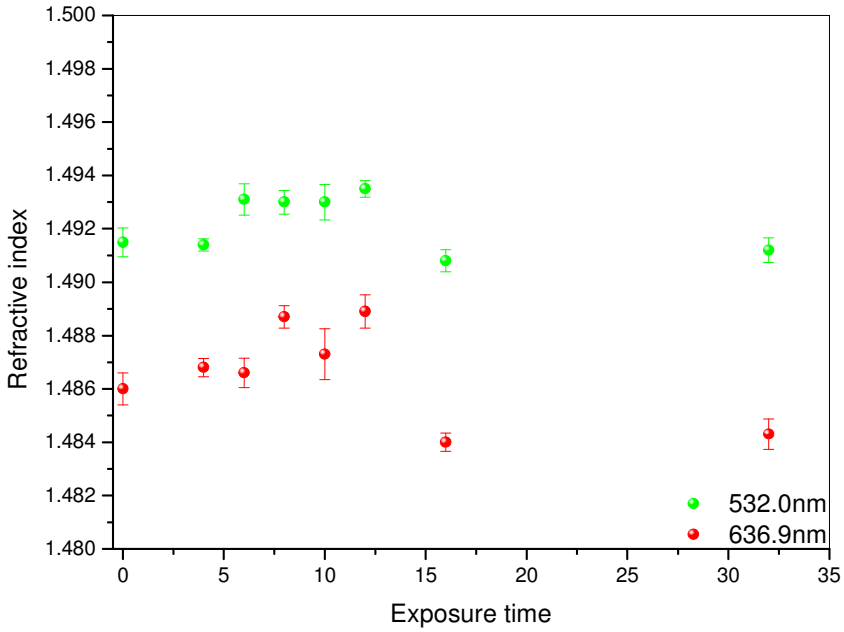

Figure 4-7 Refractive index as function of UV exposure time (Pure UPTES thin films)

- *UV exposure effect on d-UZ(600)*

As the d-UZ(600) contains photo-polymerizable compound, samples are expected to have a linear trend between the refractive index change and the UV exposure time upto to a certain limit. The linear behavior of refractive index of d-UZ(600) system is due to the photo-polymerisation of methacrylates present in the system, reported by Molina et al [4]. The change of refractive index of other hybrid systems containing Zr-oxoclusters (Zr+MAA) on UV exposure was noted to be linear [33][37]. In the following discussion, the effect of Zr and MAA concentration along with UV exposure is detailed. The varying size and shape of clusters with increasing Zr and MAA concentrations, contribute to changes in the polymerization and densification leading to different behaviors of the refractive index. For most of the samples, the changes in refractive index at 532.0 nm were higher when compared to the changes at 636.9 nm. The increase in cluster concentration (Zr+MAA) in d-UPTES and UV exposure time reduced the number of modes supported by the films. This can be explained by a reduction in the film thickness (thickness t is directly proportional to mode number). The cluster concentration also has an effect on refractive index as function of wavelength. It can be noted that the refractive index value is higher at

532.0 nm for d-UZ(600) films having same composition compared to the value at 636.9 nm. Also the refractive index variation (Δn) of a same system differs at the two different wavelengths.

The samples having various Zirconium concentrations showed different behavior on exposure to UV as discussed in the following:

- *Sample -80:20 (20% Zirconium) behavior*

The samples composing of diluted system did not show a linear behavior in refractive index change on exposure to UV. Figure 4-8 shows clearly the uneven behavior for the refractive indices of these samples. This behavior was seen in all samples containing 20% Zr with varied concentration of MAA.

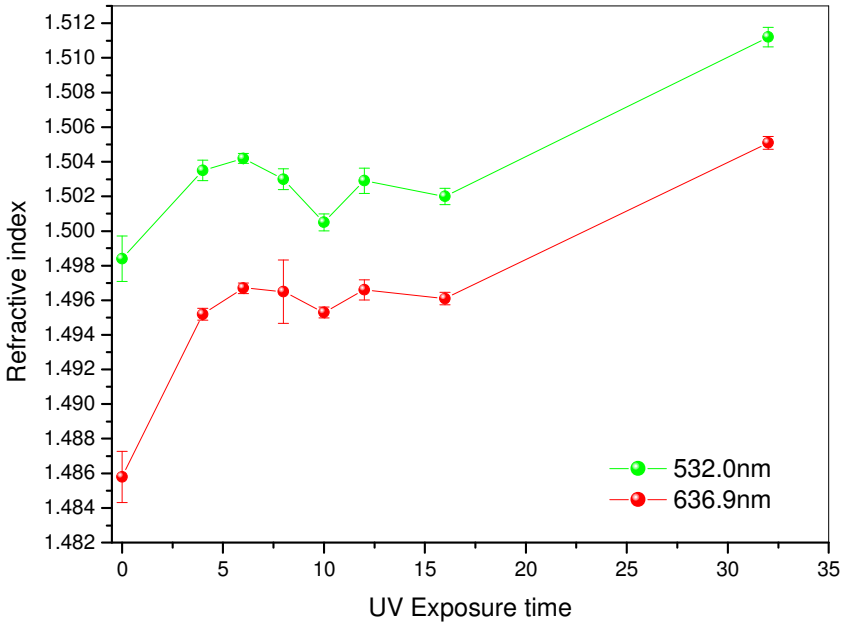

Figure 4-8 Refractive index as function of exposure time [Si:Zr:MAA 8:2:10, 2.3M]

Lines are guides for the eyes.

The reason for this behavior can be connected to the fact that at low Zr concentration the uniformity of samples is difficult to be achieved [33]. The refractive index behavior is also affected by the limitations of the measurement. At this concentration, the variation on the refractive index is small and thus the measurement error can significantly affect the results.

- *Sample -60:40 (40% Zirconium) behavior*

Samples having intermediate concentration of Zr showed linear behavior between refractive index and UV exposure. The refractive index variation with respect to UV exposure time for all samples containing 40% of zirconium with different MAA concentration, behaved in the way as shown in the figure 4-9. Table 4-4 gives coefficient results of linear fit got for this sample behavior having 2.4M of MAA.

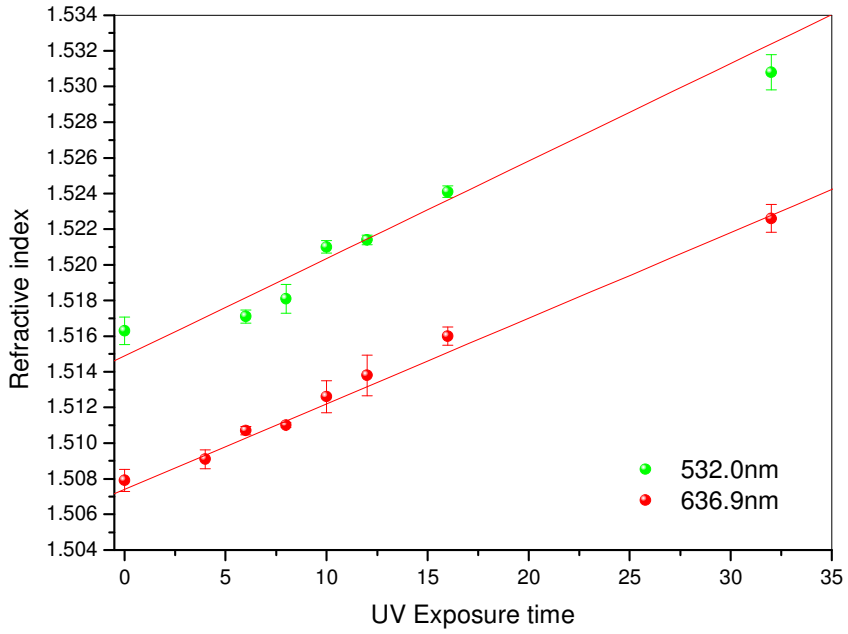

Figure 4-9 Refractive index as function of exposure time [Si:Zr:MAA 6:4:20, MAA 2.4M]

Lines are linear fittings.

Table 4-4 Linear fit results of *n* as function UV exposure time for Si:Zr 60:40, MAA 2.4M

(Linear fit [$n(t) = n_o + \Delta n \times t$])

λ(nm)	n_0	Error (n_0)	Δn (hrs^{-1})	Error (Δn) (hrs^{-1})	Correlation coefficient
532.0nm	1.5038	0.0001	0.00046	0.00008	0.9934
636.9nm	1.4970	0.0001	0.00040	0.00007	0.9943

- *Sample -40:60 (60% Zirconium) behavior:*

The behavior of refractive index with respect to UV exposure for the samples with 60% of zirconium showed exponential saturation behavior as shown in figure 4-10. The influence of concentration on cluster formation will also influence the polymerization process leading under UV irradiation. At higher concentrations, quicker and higher densification is attained. This makes these film's refractive index saturate at exposure times above 10-12 hours, which was not seen in other two concentrations. The figure 4-8 shows the behavior of the sample containing Si:Zr:MAA in ratio 4:6:30. The saturation behavior can be related to the work done by Congji Zha et al [37]. In their work, it was found that increasing the Zr concentration the saturation of refractive index change is attained faster. This clearly explains the trend of refractive index of the three different systems with different Zr concentrations and the influence of Zr on polymerization.

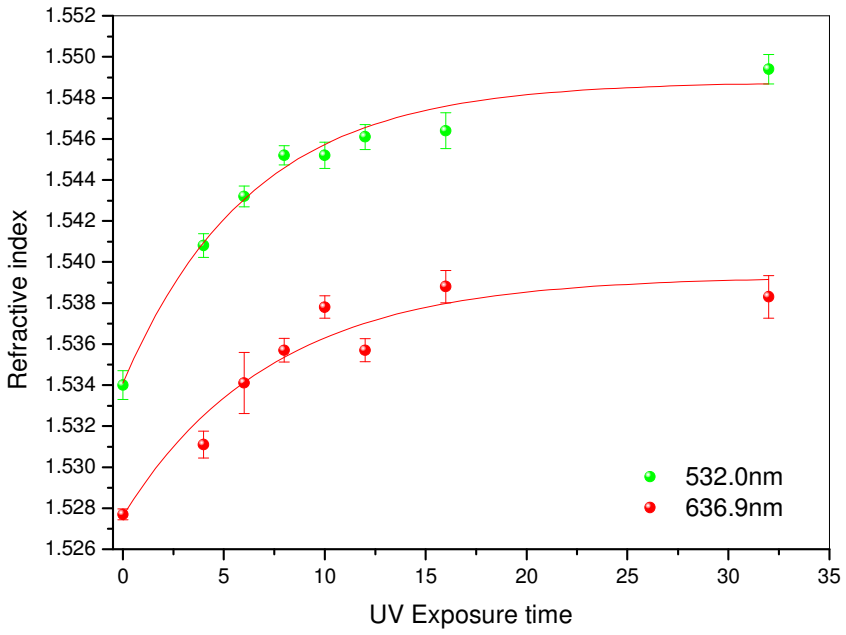

Figure 4-10 Refractive index as function of exposure time [Si:Zr:MAA 4:6:30,MAA 3.7M] Splines are exponential fitting.

The saturation behavior of sample W9 was found to exponentially increasing to a maximum value. Table 4-5 shows the exponential fit results of the expression (20).

$$n(t) = n_o + Ae^{\frac{-t}{T}} \quad \text{-- (20)}$$

where, t = exposure time, n_o = saturated value for the refractive index, A = constant coefficient and 1/T = decay constant

Table 4-5 Exponential curve fitting results of refractive indices for W9 samples

λ(nm)	n_o	Error (n_o)	A	Error (A)	T (hrs^{-1})	Error (T) (hrs^{-1})	Correlation Factor
532.0nm	1.5487	0.0006	-0.0146	0.0008	6.37	0.74	0.9819
636.9nm	1.5393	0.0009	-0.0116	0.0009	7.36	1.35	0.9658

The three different behaviors for three different concentration of Zirconium can be attributed to the cluster formation of the Zr. The different chemical reaction between Zr and MAA for cluster formation, leads to formation of clusters with different sizes. This will also affect the variation in polymerization of the cluster compound on exposure to UV. The change in polymerization which increases with concentration of cluster will change the trend of refractive index variation on UV exposure. The behaviors clearly show, higher is the cluster concentration higher is the sensitivity of the samples, quicker is the refractive index change and the saturation of refractive index change attained.

- *Absorption behavior as function of concentration change*

Figure 4-11 shows the absorption coefficient spectrum as a function of wavelength for the unexposed samples with varying MAA concentration. Color lines in the figure 4-11 correspond to different samples. For clear understanding absorption coefficient values at 255 nm is used. Table 4-6 gives the absorption coefficient values for d-UZ(600) systems at 255 nm wavelength.

The different behavior of refractive index evolution can be explained with the UV absorption behavior of the unexposed samples. The absorption spectrum and study on the absorption behavior of the unexposed sample was done to know the cluster concentration influence on UV absorption which is directly related to refractive index change.

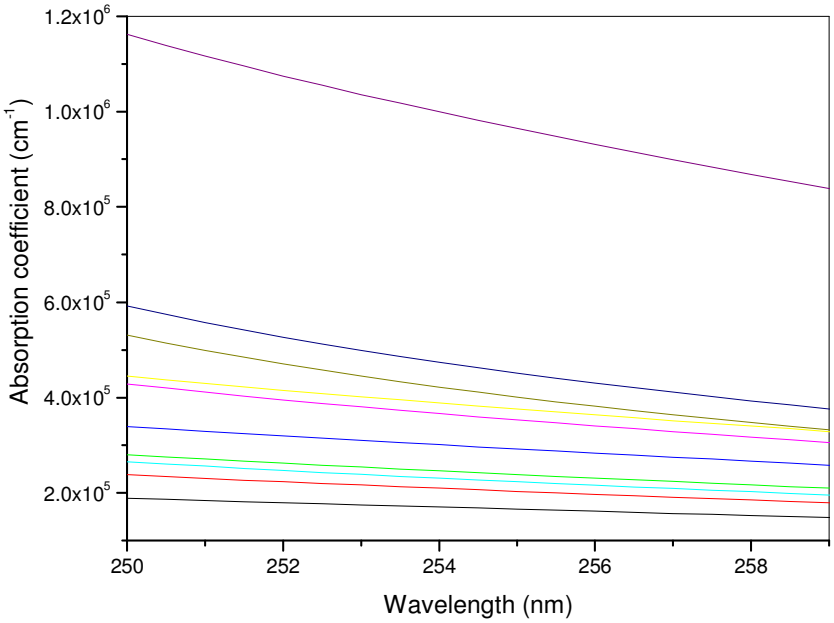

Figure 4-11 Absorption coefficient as function of wavelength

Table 4-6 Absorption coefficient values of all unexposed samples at 255nm

Wavelength (nm)	Absorption coefficient $\times 10^4$ (cm^{-1})	Sample
255	16.60	W0
255	20.33	W2
255	23.87	W3
255	29.23	W4
255	22.34	W5
255	35.32	W6
255	37.59	W7
255	40.10	W8
255	45.13	W9
255	96.46	W10

The absorption is dependent on the SiO_2, ZrO_2 and MAA species present in the system. As we can see that at higher concentrations of d-U(600) the absorption is low even with the presence of clusters. So the influence of SiO_2 and other species of d-U(600) can

be neglected as compared to the cluster compounds. As stated in [38], completely oxidized Zirconia films exhibit low absorption between 250 nm and to atleast 10 μm. But the influence of Zirconium dioxide on absorption cannot be neglected. The change in absorption coefficient values between W4 and W6 samples (containing similar MAA concentration) is 20%. This shows increase in Zr in system, increases absorption, which directly affects the photopolymerisation process. As explained by Ceng Dong et al [39], photopolymerization of methyl methacrylate containing nanosized titanium dioxide is influenced by TiO_2 concentration change. This can be correlated to the high increase of the absorption coefficient with the Zr concentration. The Zr concentration increase leads to quicker change in refractive index and a faster saturation of the refractive index change. This is due to the fact that polymer length increases with Zr concentration which increases the rate of polymerization. Thus Zr concentration indirectly increases the absorption of the system by increasing the length of the polymers.

The main cause of the absorption variation is the concentration change of the methacrylate species (MAA concentration). It can be said that the absorption of system depends mainly on propoxy, methacrylate and hydroxyl ligands present in the cluster along with Zr. The absorption coefficient observed for the diluted and intermediate system shows that the influence of MAA is higher than Zr concentration. As the MAA concentration increases, the value of the absorption coefficiency also increases in all the three systems. But comparing Δn (refractive index slope) with the absorption coefficient value, we can say that Zr has high influence on the Δn values, whereas MAA influence on Δn is not significant.

As we have systems of varied cluster concentration, the cluster concentration influence on the absorption and Δn can be explained from the results. It is noticed that when the cluster concentration increases, it increases the absorption of the system and also increases Δn.

- *Limitations of absorption measurement*

The absorption spectrums of the samples were obtained by Jasco instrument (Model V-560) in which absorbance is calculated by the Beer-Lambert law, measuring the incident and transmitted intensities of the light signal. However, Beer Lambert law is valid only if the absorbing species are independent of each other and if the absorption occurs in a

uniform medium [40], which is not true for the systems under consideration. This can be said because MAA polymerization is influenced by Zirconium oxide as stated before. As well the system's cluster concentration is not uniform for certain samples containing low Zr concentrations [33]. Also in the Beer-Lambert formula the effect of reflection and scattering of the sample is not included. Thus, the values of the absorption coefficients can only be taken as an approximate value for explaining the effect of concentration of Zr and MAA on the system.

4.4 Comparison of material influence on exposure to UV irradiation

Table 4-7 gives the coefficients for the linear fit of the refractive index value as function of the UV exposure time, measured at 532.0 nm and 636.9 nm.

The fit values are derived from the equation,

$$n(t) = n_o + \Delta n \times t \quad \text{-- (22)}$$

$$n(E) = n_o + \Delta n' \times E \quad \text{-- (23)}$$

n_o = intial refractive index value (unexposed sample), $n(t)$ = refractive index value with respect to exposure time given by t, $n(E)$ = refractive index value with respect to UV exposure energy given by E, Δn = coefficient of rate of refractive index change as function of time, $\Delta n'$ = coefficient of rate of refractive index change as function of energy

Except for W9 samples, all refractive indices of respective samples were plotted including the refractive index value corresponding to 32 hours UV exposure time. Refractive index change started showing saturation for W9 samples at a lower exposure time as compared to other samples having Zr in lower concentration (for other samples saturation of refractive index was not seen until 32hrs of UV exposure). This behavior was expected, since increasing Zr content reduces the time for refractive index to attain saturation limit [37].

For samples containing low zirconium (80:20(Si:Zr)), refractive index values at certain times were only chosen to get a better fit and to estimate an approximate linear behavior. The correlation factor for samples W5, W6 and W7, shows that the behavior of these samples can be reported as linear. Other samples show low values for correlation factor. The influence of precursor concentration on UV exposure is discussed in the following.

Table 4-7 Linear fit (coefficient) values for *n* as function of UV exposure time in hrs.

λ(nm)	Sample	n_o Initial *n*	Error (n_o)	Δn	Error (Δn)	Correlation Factor
532.0nm	W1	1.4995	0.0004	0.00027	0.00002	0.9470
	W2	1.4973	0.0004	0.00040	0.00002	0.9197
	W3	1.5012	0.0002	0.00035	0.00002	0.9929
	W4	1.4973	0.0001	0.00043	0.00009	0.9746
	W5	1.5038	0.0001	0.00046	0.00008	0.9934
	W6	1.5143	0.0003	0.00058	0.00003	0.9841
	W7	1.5210	0.0001	0.00047	0.00001	0.9797
	W9*	1.5363	0.0005	0.00095	0.00006	0.9281
636.9	W1	1.4933	0.0003	0.00020	0.00001	0.9450
	W2	1.4899	0.0003	0.00046	0.00002	0.9733
	W3	1.4955	0.0003	0.00041	0.00003	0.9526
	W4	1.4937	0.0002	0.00032	0.00002	0.9597
	W5	1.4970	0.0001	0.00040	0.00007	0.9943
	W6	1.5073	0.0002	0.00048	0.00002	0.9841
	W7	1.5123	0.0009	0.00056	0.00007	0.9996
	W9*	1.5279	0.0002	0.00085	0.00004	0.9761

W9* - For W9 samples refractive index values were chosen for exposure times 0, 4, 6, 8, 10 and 12 hrs.

- *UV exposure + Zirconium influence*

Figure 4-12 and 4-13 shows the evolution of refractive index with respect to UV exposure in accordance to Zr concentration increase, measured at 532.0 nm and 636.9 nm respectively. The refractive index of the samples W4 and W6, those having close amounts of MAA concentration are being considered for this discussion, to study the Zirconium effect on Δn of the films exposed to UV. It clearly show that the refractive index change (Δn) as the function of exposure time is highly influenced by the concentration of Zr. One of the main reasons is that Zirconium dioxide assists the polymerization of the methacrylates by increasing the photosensitivity [37]. The results show that Δn increases with Zr concentration and higher the Zr concentration quicker is the time to attain saturation.

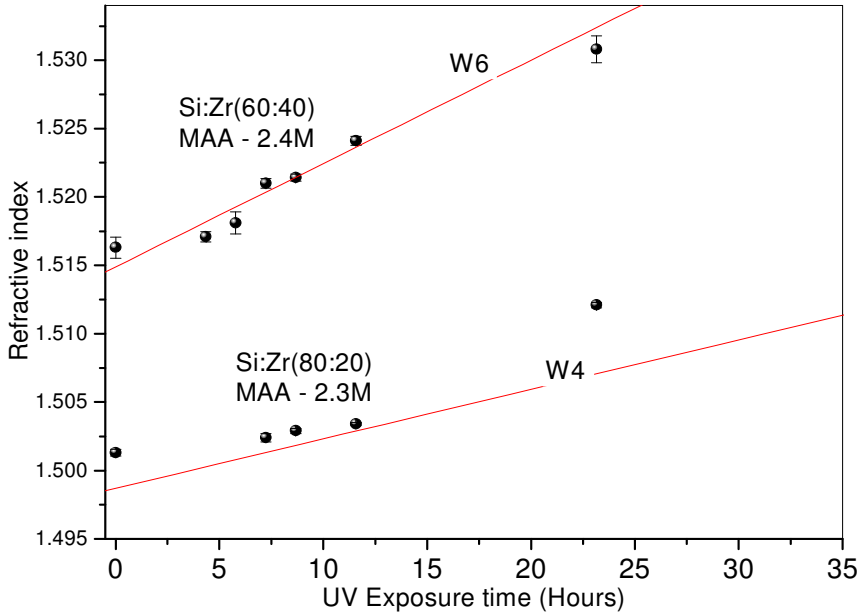

Figure 4-12 Refractive index as a function of Zr concentration (UV exposed) @ 532.0 nm of W4 and W6. Lines are linear fit.

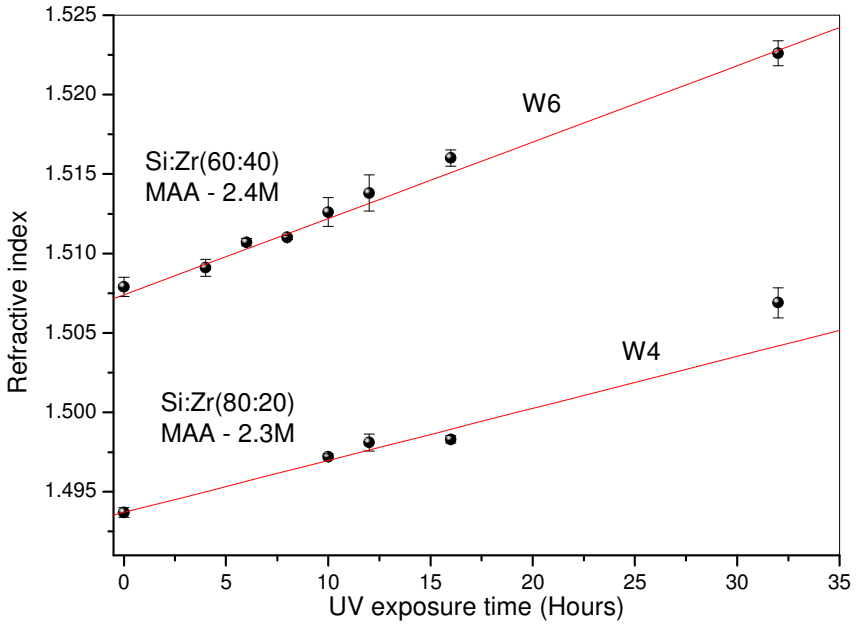

Figure 4-13 Refractive index as a function of Zr concentration (UV exposed) @ 636.9 nm of W4 and W6 samples. Lines are linear fit.

From the figures 4-12 and 4-13 it is clear that controlling Zr along with UV exposure time, higher range of refractive index can be attained with higher accuracy. At concentration of 40% of ZPO in 60% of d-UPTES good linearity in the variation of refractive index is noticed. Thus at this concentration and close to this concentrations controlled refractive index change can be attained.

UV exposure + Methacrylic acid influence:

Figure 4-14 and 4-15 shows the evolution of refractive index with respect to UV exposure as a function of MAA concentration at 532.0 nm and 636.9 nm respectively.

The increase in the methacrylic acid contributes to the increase in the system's response to UV. From the figures 4-14 and 4-15, it can be seen that increasing the MAA concentration the gap between the refractive index values of different samples is reduced. This behavior is more similar to the behavior noted in unexposed samples, which shows a saturation behavior as the concentration of MAA increase.

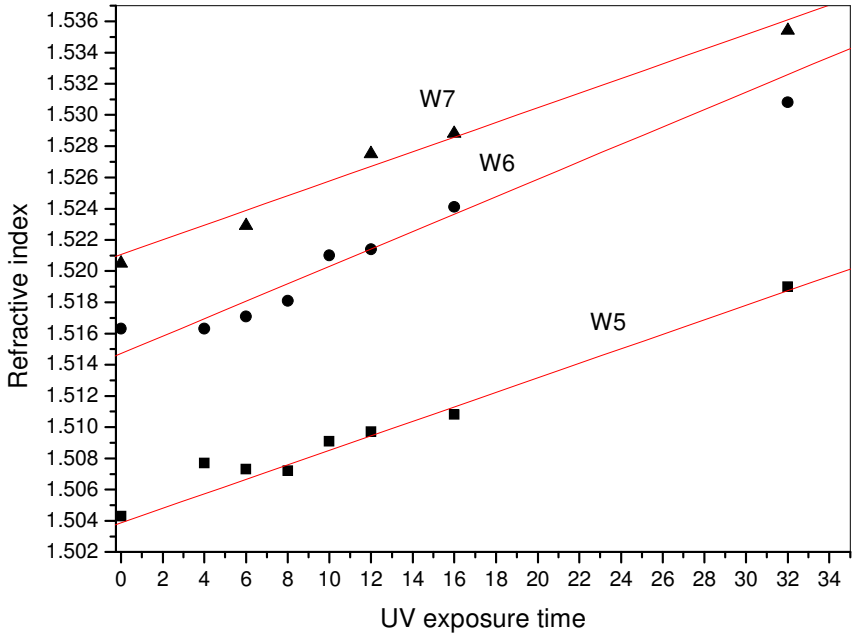

Figure 4-14 Refractive index as a function of MAA concentration [Si:Zr-60:40(UV exposed)] @ 532.0 nm of W5, W6 and W7 samples. Lines are linear fit.

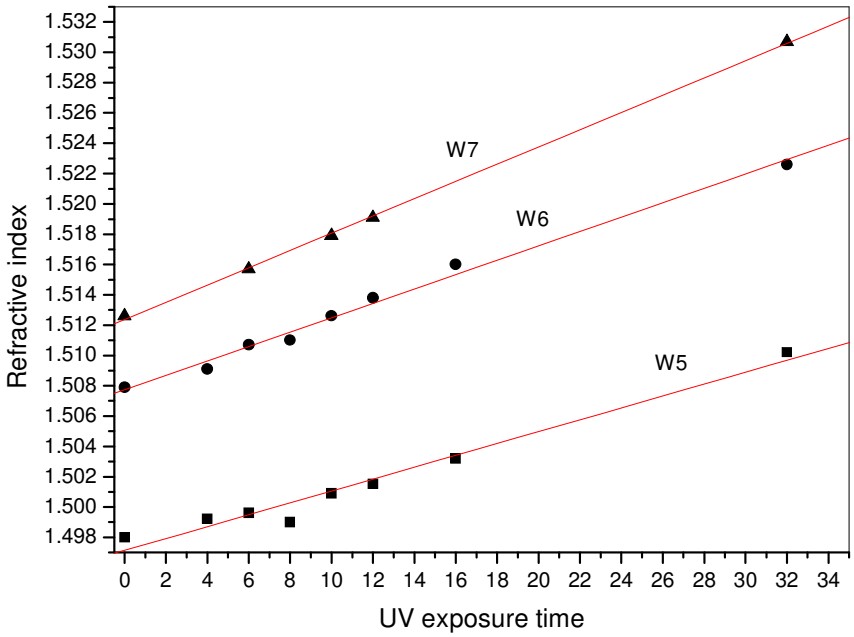

Figure 4-15 Refractive index as a function of MAA concentration [Si:Zr-60:40(UV exposed)] @ 636.9 nm of W5, W6 and W7 samples. Lines are linear fit.

Figures 4-14 and 4-15 show the change of refractive index is much higher as we move from 0.4M to 2.5M of MAA concentration as compared to refractive index change when moving from 2.5M to 4M MAA concentration in the system. This confirms that above a certain concentration of MAA the system's refractive index could not be changed. Comparing influence of Zr and MAA concentrations on the increase of refractive index, Zr has more influence than MAA. The increase in Zr concentration leads to increase in the refractive index value. The higher increase in MAA concentration shows saturation of the refractive index values.

UV exposure + Cluster concentration influence:

Since the clusters consist of ZPO and MAA moities bonded together, it is necessary to know the refractive index dependence on cluster concentration. It is also important to know the cluster concentration influence and the polymerization length (also size and shape of the clusters) to explain clearly the refractive index dependence. The photo-polymerizations with varying ZPO and MAA concentration will change the cluster concentration as well as the size and shape of the cluster which in turn changes the

refractive index behavior. For this analysis we can take the samples W4 and W6 for discussion, which were used for the Zr concentration influence. The concentration of clusters in sample W6 will be higher than that of W4 as the ZPO and MAA concentration are higher in sample W6. The refractive index values as well as the change in the refractive index (Δn) are very high for the W6 samples. This clearly suggests that, the refractive index value grow with the cluster concentration and higher is the rate of attaining the refractive index changes on exposure to UV. This also suggests that cluster concentration will increase the length of polymers and also the densification of samples. Here it must be also taken into account the refractive index trend of the system containing low cluster concentration (dilute system) was not linear to UV exposure. This means that the Zr-oxo-cluster concentration behavior on exposure to UV as stated here only explains the behavior of systems containing intermediate concentration to higher concentration. Figures 4-16 and 4-17, showing 3-D graph plotted for refractive index as function of MAA concentrations and UV energy for samples having Si in UPTES and Zr in ZPO in ratio 60:40, shows clearly the effect of cluster concentration and UV exposure energy.

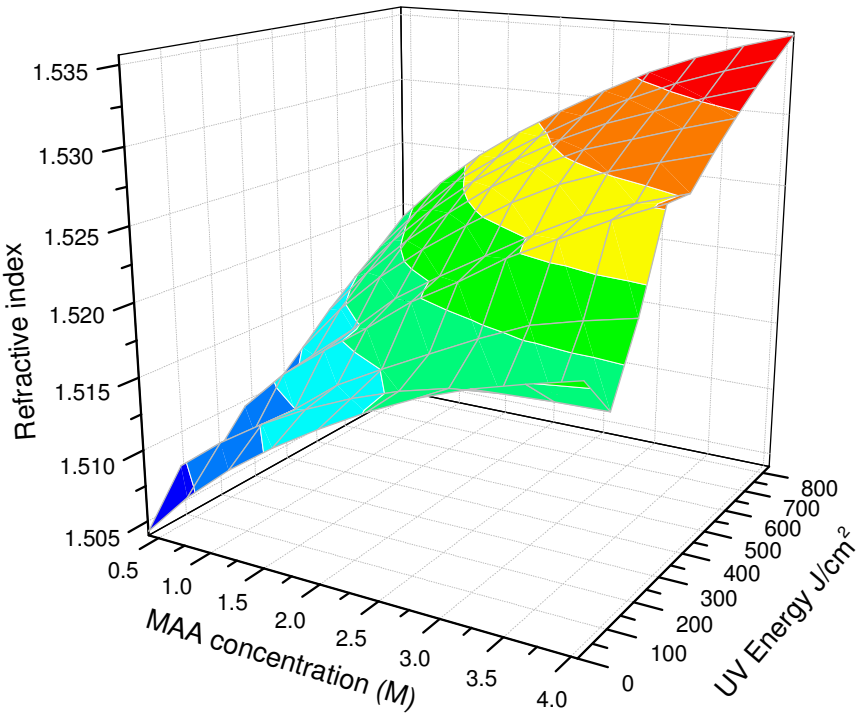

Figure 4-16 *3-D plot* ***n*** as function of MAA concentration and Energy dose at 532.0 nm

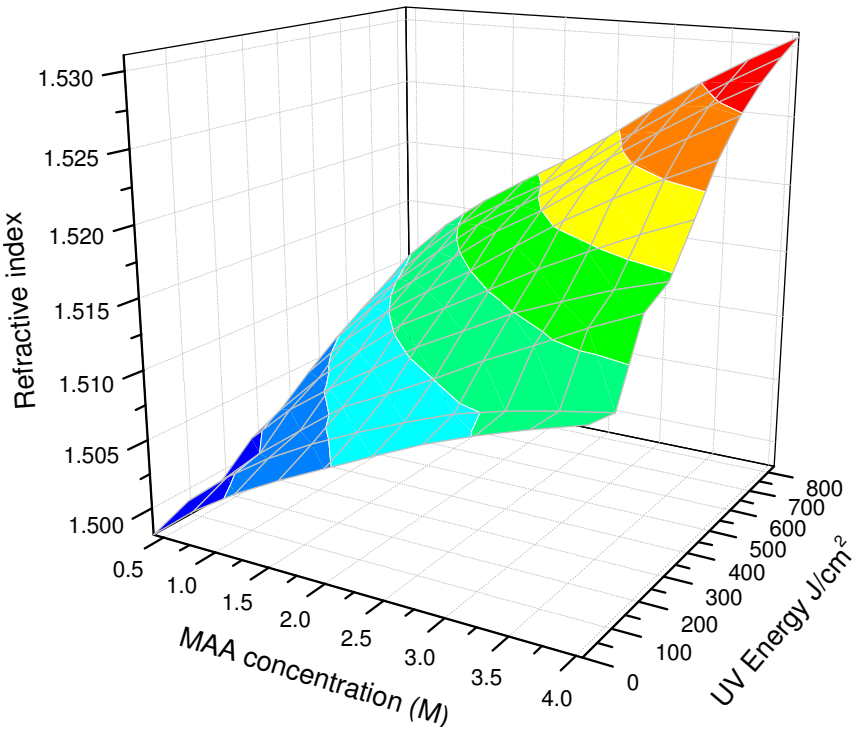

Figure 4-17 *3-D plot* ***n*** as function of MAA concentration and Energy dose at 636.9 nm

5. CONCLUSION AND FUTURE WORK

5.1 Conclusion

Organic-inorganic hybrid materials under research are showing considerable potential for use in processing of integrated optical devices for optical telecommunication. Studies are showing that these materials can be processed easily, are available at low cost and have many advantages over other currently used materials for integrated optical device fabrication. The hybrid material classed as 'di-ureasil Zirconium oxocluster' has shown that it has all the necessary properties to be considered as a potential material for the fabrication of integrated optical devices.

In this work, the refractive index of thin films made of the di-ureasil Zirconium oxo-cluster materials were studied as a function of precursor concentration and UV exposure time. Sol-gel and spin coating techniques were used to produce the di-ureasil Zirconium thin films in varied concentrations. The concentration change was made with respect to molar percentage of Si and Zr along with varying MAA content. This was done to get films of various compositions of d-UPTES and MAA modified Zr-oxoclusters. The films were exposed to UV irradiation for various times. The refractive indices of the unexposed samples and the UV exposed samples were measured using the prism coupler technique.

The steps involved in the sol-gel and spin coating to process thin films of d-UZ(600) material are reported. The analysis on refractive index as a function of Zr and MAA content and UV irradiation are done in this work. The study showed that higher range of refractive index changes without UV exposure could be achieved by addition of Zr, however, very high ZPO content leads to precipitation and higher scattering which makes sample not viable for IO device fabrication. The results showed the MAA addition plays an important role in the refractive index changes on exposure to UV, as it increases the refractive index due to photo-polymerization. But higher concentrations of MAA also lead to unusable or low efficient samples for IO device fabrication due to surface roughness and scattering. It was noted that intermediate concentration (having ratio of Si:Zr in 60:40) is best suited for precise refractive index changes and to process IO devices.

The UV exposure sensitivity of the three different systems was found to be different. The lowest sensitivity value (Δn) was found for W1 (diluted system with very low MAA concentration) samples. The results clearly showed that increase in the cluster concentration will increase the sensitivity of the system to UV exposure, leading to quicker change in refractive index. Good optical quality and easy tunability of refractive index, make the intermediate system among the three systems, the best suited for waveguide processing and optical telecommunication application.

The tunability of refractive index of the diluted system (Si:Zr - 80:20) and the higher concentrated system (Si:Zr - 40:60) is difficult due to presence of higher cluster concentration. At intermediate concentrations (Si:Zr - 60:40) with varying MAA in molar ratio, the tunability using concentration change of material (unexposed films) was easily attained. As well there was linear behavior of this system's refractive index change on UV exposure. From the study it can be concluded that, thin films containing intermediate concentrations (Si:Zr - 60:40) with varying MAA can be used to process IO devices such as channel waveguide, planar waveguide, couplers, multiplexers, filters, etc. As the cluster formation is said to be good at a concentration ratio of 1:2 for Zr and MAA, the films at these compositions ought to have good optical properties.

5.2 Future work

Further study on refractive index at infra red wavelengths (@1550nm) should be done. The polymerization of ZPO with low concentrations of methacrylic acid must be studied in order to know the chemical kinetics, since it was noticed that the precipitation disappeared after long time from the preparation of Sol and thin films having Si, Zr and MAA in ratio 8:2:1 were processed which was not expected as the MAA concentration is very low to stabilize Zr at this ratio. This study is to be done because it is significant that less use of MAA will increase the device efficiency. Absorption effects should be studied on the system by effective spectrometry like the FT-Raman spectroscopy to study the effect of concentration of precursors and to conclude to better proportions of Zr and MAA, to get an optimum slope for refractive index variation. The study on IO devices prepared at the intermediate concentration (*i.e.* Si:Zr - 60:40 and systems having concentrations close to this system) with varying MAA concentration from 2M to 5M must be done to know the best MAA content for this system.

6. REFERENCE

[1] S.I.Najafi. *Introduction to glass integrated optics,* Artech House, London, 1992.

[2] C.Vicente, E.Pecoraro, R.A.Sá.Ferreira, P.Andre, R.Nogueira, Y.Messaddeq, S.Ribeiro, L.D.Carlos. *Waveguides and gratings fabrication in zirconium-based organic/inorganic hybrids.* J Sol-Gel Sci Technology 48 (2008) 80-85.

[3] E.Pun and W.H.Wong.*Polymeric waveguides and devices for integrated optics applications*. www.ursi.org/Proceedings/ProcGA02/papers/p0546.pdf [online] [cited: 07.09.09]

[4] C.Molina, P.J.Moreira, R.R.Gonçalves, R.A.Sá.Ferreira, Y.Messaddeq, S.J.L.Ribeiro, O. Soppera, A.P.Leite, P.V.S.Marques, V.Bermudez and L.D.Carlos. *Planar and UV written channel optical waveguides prepared with siloxane–poly(oxyethylene)–zirconia organic–inorganic hybrids. Structure and optical properties.* Mater. Chem. 15(2005) 3937.

[5] P.Ayras, J.T.Rantala, S.Honkanen, S.B.Mendes, N.Peyghambarian. *Diffraction gratings in sol–gel films by direct contact printing using a UV-mercury lamp.* Optics Communications 162 (1999) 215-218.

[6] C.Xu, L.Eldada, C.Wu, R.A.Norwood, L.W.Shacklette, and J.T.Yardley. *Photoimageable, Low Shrinkage Organic-inorganic hybrid materials for practical multimode channel waveguides.* Chem. Mater. 8 (1996) 2701-2703.

[7] R.Buestrich, F.Kahlenberg and M.Popall. *ORMOCERs for Optical Interconnection Technology.* Journal of Sol-Gel Science and Technology. 20(2001) 181–186.

[8] A.A.Bettiola, S.V.Rao, T.C. Suma, J.A.Kana and F.Watta. *Fabrication of optical waveguides using proton beam writing.* 288 (2006) 209–212.

[9] K.Tamaki, H.Tekase, F.Huang, Y.Eriyama, T.Ukachi. *Development of photosensitive organic-inorganic hybrid materials with high resolution for optical splitters.* 16 (2003) 203-208.

[10] http://www.metricon.com/ellip.htm. [online] [cited: 07.09.09]

[11] K.Chiang, S.Cheng, and Q.Liu,. *Characterization of Ultrathin Dielectric Films With the Prism-Coupler*. Method Journal of lightwave technology. 25(2007)1206.

[12] R.Ulrich, Torge. *Measurement of thin film parameters with a prism coupler.* R. Applied Optics IP. 12(1973)2901.

[13] http://en.wikipedia.org/wiki/Waveguide_(optics). [online] [cited: 07.09.09]

[14] http://www.rp-photonics.com/waveguides.html. [online] [cited: 08.09.09]

[15] H.Nishihara, M.Haruna, T.Suhara. *Optical integrated circuit.* McGraw-Hill Optical and Electro-Optical Engineering Series, 1989.

[16] G.Kickelbick. *Hybrid Materials Synthesis, Characterization, and Applications,.* Wiley-VCH. 2007.

[17] Rapún, N. *Packaging Materials: Organic–Inorganic Hybrids for Millimetre-Wave Optoelectronics.* Materials for Information Technology. Springer London. (2005) 391-404 http://www.springerlink.com/content/pr002187vm041735/ [online] [cited: 08.09.09]

[18] D.C.Oliveira, A.G.Macedo, N.J.O.Silva, C.Molina. *Photopatternable Di-ureasil-Zirconium Oxocluster Organic-Inorganic Hybrids As Cost Effective Integrated Optical Substrates.* Chem. Mater. 20(2008)3696–3705.

[19] U.Schubert. *Polymers Reinforced by Covalently Bonded Inorganic clusters.* Chem Mater. 13(2001)3487-3494.

[20] U.Schubert, G.Kickelbick. *Inorganic Clusters in Organic Polymers and the Use of Polyfunctional Inorganic Compounds as Polymerization Initiators.* Monatshefte fur Chemie. 132(2001)13-30 .

[21] Rajendra K.Krishnaswamy, Jay Janzen, *Exploiting refractometry to estimate the density of polyethylene: The Lorentz-Lorentz approach revisited,* Polymer Testing 24(2005)762-765.

[22] Ahrens, L. H., *Variation of refractive index with ionization potential in some isostructural crystals*. Mineral. Mag. 81(1958)929-936.

[23] C.Jeffrey Brinker, George.W.Scherer,. *Sol-Gel science, Physics and Chemistry of SOL-GEL processing.* Academic press Inc., 1990.

[24] *http://www.psrc.usm.edu/mauritz/solgel.html.* [online] [cited: 08.09.09]

[25] *http://www.apexicindia.com/SpinCoatingTheory.htm.* [online] [cited: 08.09.09]

[26]*http://classes.engr.oregonstate.edu/cbee/winter2005/che414/Honors/Spin%20Coating.ppt* . [online] [cited: 08.09.09]

[27]*http://www.sciner.com/DelMarPhotonics/GreyhawkOptics/rutile_laser_tuning.htm*

[28]Hiromitsu Kozuka, Kansai University, Suita, Osaka, Japan,. *Handbook of Sol-Gel Science and Technology Processing, Characterization and Applications.* Vol I. Kluwer Academic Publishers.

[29] http://teaching.shu.ac.uk/hwb/chemistry/tutorials/molspec/uvvisab1.htm. [online] [cited: 27.11.09]

[30] http://www.chemguide.co.uk/analysis/uvvisible/bonding.html#top. [online] [cited: 27.11.09]

[31] http://www.orc.soton.ac.uk/viewpublication.html?pid=2359, Pogress in photosensitivity of glasses - fundamentals and overview, Heike Ebendorff-Heidepriem. [online] [cited: 27.11.09]

[32] F.Vasco, *Ferramentas de caracterização de guias de onda planares[Thesis]*, Departamento de fisica, University of Aveiro, 2008.

[33] X.Zhang, H.Lu, A.M. Soutar and X.Zeng. *Thick UV-patternable hybrid sol-gel films prepared by spin coating.* Journal of Material Chemistry, 14(2004)357-361.

[34] S. Deki, H.Y.Y.Ko, T.Fujita, K.Akamatsu, M.Mizuhata, and A.Kajinami. *Synthesis and microstructure of metal oxide thin films containing metal nanoparticles by liquid phase deposition (LPD) method.* The European Physical Journal. (2001)325-328.

[35] K.Luo, S.Z.Limin. *High refractive index and good mechanical property UV-cured hybrid films containing zirconia nanoparticles.* Thin Solid Films 517(2009)5974–5980.

[36] A. Ovsianikov, A. Gaidukeviciute, B. N. Chichkov, M. Oubaha, B. D. MacCraith, I. Sakellari, A. Giakoumaki, D. Gray, M. Vamvakaki, M. Farsari and C. Fotakis. *Two-Photon Polymerization of Hybrid Sol-GelMaterials for Photonic application.* Laser Chemistry, 2008.

[37] C.Zha, X.Luo, R.Wang, B.L.Davies. *Effects of TiO2 and ZrO2 on optical properties of organic–inorganic hybrid polymers and thin films.* Journal of Mater Science: Mater Electron. 18(2007) S331–S334.

[38] www.cerac.com/pubs/proddata/zro2.pdf. [online] [cited: 08.09.09]

[39]C.Dong, X.Ni. *The photopolymerization and Characterizatoin of Methyl Methacrylate Initiated by Nanosized Titanium Dioxide.* Journal of Macromolecular Science. A41 (2004)547-563.

[40] http://www.andor-tech.com/learn/applications/?docID=189. [online] [cited: 08.09.09]

7. APPENDIX

Appendix A: Absorption behavior

Figure A1 shows the complete UV-Visible spectrum of the unexposed sample. No absorption was noted in the boron silicate substrate spectrum (not shown in the figure). The substrate is transparent to entire UV-Visible wavelengths. Since the source UV wavelength peak is at 255 nm, the entire spectrum is not significant for the thesis.

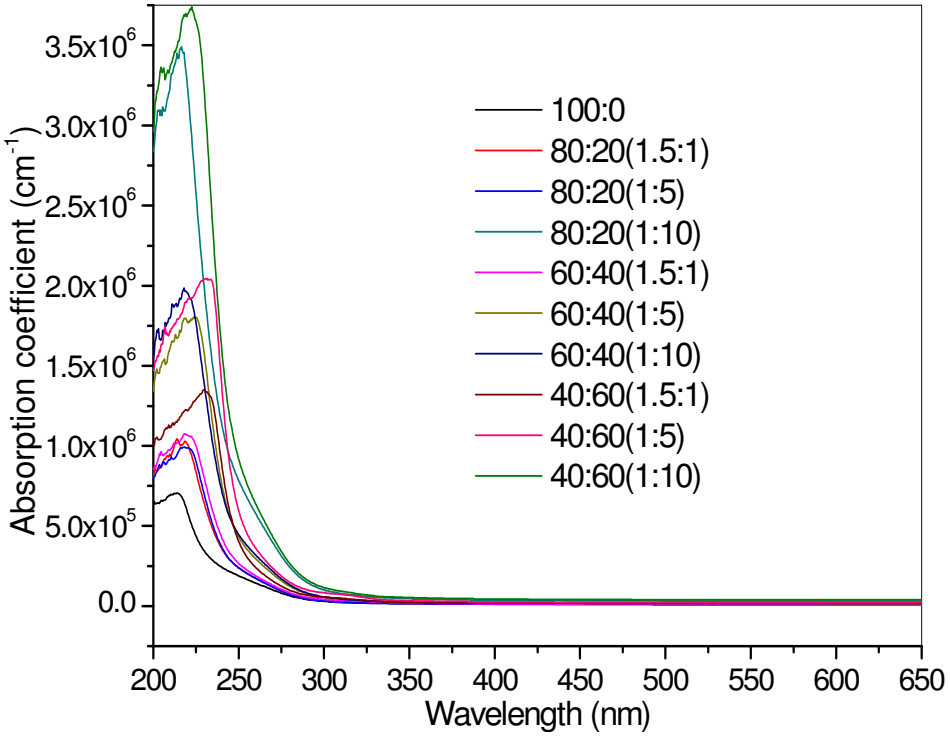

Figure-A1 UV-Visible spectrum of unexposed thin film samples

In Figure-A2 absorption coefficient at 255 nm values of unexposed samples plotted against MAA concentration shows clearly the Zr and MAA influence on absorption. The values of the absorption coefficients are tabulated in the results and discussion part.

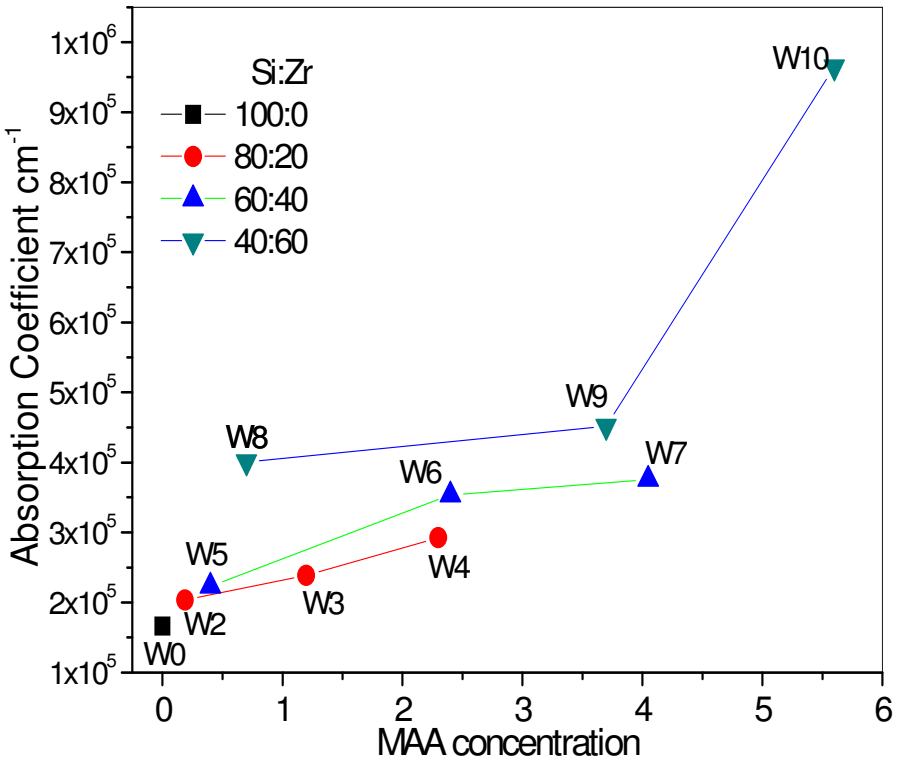

Figure-A2 - Absorption coefficient vs Zr and MAA concentration